© 2017. Published by The Company of Biologists Ltd | Journal of Cell Science (2017) 130, 3374-3387 doi:10.1242/jcs.200170

RESEARCH ARTICLE

The armadillo protein p0071 controls KIF3 motor transport

Alexander Becher[1,*], Tim Eiseler[1,*], Marc Porzner[1], Paul Walther[2], René Keil[3], Susanne Bobrovich[1], Mechthild Hatzfeld[3] and Thomas Seufferlein[1,‡]

ABSTRACT

We here report a novel function of the armadillo protein p0071 (also known as PKP4) during transport mediated by the KIF3 transport complex. Secretion of chromogranin A and matrix metallopeptidase 9 from pancreatic neuroendocrine tumor cells or pancreatic cancer cells, respectively, was substantially reduced following knockdown of p0071. Vesicle tracking indicated that there was impaired directional persistence of vesicle movement upon p0071 depletion. This suggests a disturbed balance between plus- and minus-end directed microtubule transport in cells lacking p0071. p0071 directly interacts with the KIF3 motor subunit KIF3B. Our data indicate that p0071 also interacts with the kinesin cargo adaptor protein KAP3 (also known as KIFAP3) acting as a stabilizing linker between KIF3B and its KAP3 cargo-binding entity. Thus, p0071 is required for directional vesicle movement and secretion of different KIF3-transported carriers, thereby regulating the transport of intracellular membrane vesicles along microtubules.

KEY WORDS: p0071, Chromogranin, MMP9, Kinesin-2, KIF3, Protein transport

INTRODUCTION

The protein p0071 (also known as plakophilin 4, PKP4), p120-catenin (also known as CTNND1), NPRAP (also known as CTNND2), ARVCF and the more distantly related plakophilins 1–3 (PKP1, PKP2 and PKP3) belong to the p120 family of armadillo repeat proteins (McCrea and Gu, 2010). p120 catenins act as scaffolds in large protein complexes and contain an array of 40–45 amino acid sequence repeats, the so-called armadillo (arm) repeats (Alema and Salvatore, 2007; Keil et al., 2013; Schackmann et al., 2013). In addition, p0071 also harbors a PDZ domain at its C-terminal end (Keil et al., 2013). p0071 has been implicated in various cellular processes, including intercellular adhesion, neurite outgrowth, cytoskeletal organization, cell division (Keil et al., 2007; Nolze et al., 2013; Wolf et al., 2006) and Rab11-dependent endosomal recycling (Keil and Hatzfeld, 2014). p0071 contributes to these cytoskeleton-dependent processes by controlling Rho GTPase signaling. Upon interaction with RhoA and the RhoGEF Ect2, p0071 was shown to foster contractile ring formation/maintenance during mitosis. Both, knockdown or high ectopic expression of p0071 resulted in mitotic dysregulation (Keil et al., 2013; Wolf et al., 2006).

Intracellular transport of p0071 to the midbody or adhesion sites, as well as proper localization of p0071 during cell division, depends on the microtubule cytoskeleton and is mediated by direct interaction with the kinesin protein KIF3B. KIF3B is a motor subunit of the anterograde heterotrimeric KIF3 transport complex, which belongs to the kinesin-2 family and comprises KIF3A, KIF3B and the cargo adaptor protein KAP3 (Keil et al., 2009, 2013; Verhey and Hammond, 2009). KAP3 preferentially binds the C-terminal rod of the KIF3A–KIF3B heterodimer and promotes the efficient binding of membranous cargo vesicles (Deacon et al., 2003; Jimbo et al., 2002; Takeda et al., 2000). In contrast to vesicle-packaged cargo proteins, the interaction of p0071 with KIF3B was shown to be independent of KAP3 (Keil et al., 2009). Additional functions of the p0071–KIF3 complex are as yet elusive.

Apart from its function regulating mitosis, the KIF3 complex is involved in many fundamental biological processes. In non-neuronal mammalian cells, this complex transports membranous cargo vesicles between the endoplasmatic reticulum and the Golgi complex (Stauber et al., 2006). Altered vesicular sorting or transport of specific cargos has been repeatedly linked to various types of cancer and therefore represents a potential target for therapeutic interventions (Patel et al., 2014). The KIF3 complex is also implicated in the transport of dense core granules towards the plasma membrane (Scholey, 2013). Trafficking of dense core vesicles has been previously investigated in BON cells, a cell line established from a human pancreatic neuroendocrine tumor (NET) (Evers et al., 1994; von Wichert et al., 2005). BON cells are of neuroectodermal origin and exhibit hypersecretion of various substances that include bioamines and neuropeptides, such as IGF-I or the secretogranin Chromogranin A (CgA) (von Wichert et al., 2005, 2000). CgA is also an important marker of NETs *in vivo*. The secretion of CgA can therefore serve as a tool to monitor the molecular mechanisms of protein transport from the trans-Golgi network (TGN) to the plasma membrane.

The involvement of p0071 in processes associated with cytoskeletal organization as well as its direct interaction with KIF3B, prompted us to investigate whether p0071 also contributes to intracellular transport of membranous cargo vesicles.

RESULTS

p0071 colocalizes with microtubules and CgA vesicles in pancreatic neuroendocrine cancer cells

p0071 is ubiquitously expressed and is primarily detectable at cellular adhesion sites, but also seen in the cytoplasm and the perinuclear area (Hatzfeld, 2005; Hatzfeld and Nachtsheim, 1996; Jakobsen et al., 2013; Wolf et al., 2006). In line with these data, immunofluorescence analysis of endogenous p0071 in BON cells demonstrated localization to adhesion contacts as well as strong cytoplasmic and perinuclear signals (Fig. 1A). There was no specific colocalization with the perinuclear trans-Golgi marker

[1]Department of Internal Medicine I, Ulm University, Albert-Einstein-Allee 23, 89081 Ulm, Germany. [2]Central Facility for Electron Microscopy, Ulm University, Albert-Einstein-Allee 11, 89081, Ulm, Germany. [3]Institute of Molecular Medicine, Division of Pathobiochemistry, Martin-Luther-University of Halle-Wittenberg, D-06114 Halle, Germany.
*These authors contributed equally to this work

‡Author for correspondence (Thomas.seufferlein@uniklinik-ulm.de)

A.B., 0000-0003-1552-1581; T.E., 0000-0001-7819-4659; T.S., 0000-0003-3259-0810

Received 30 November 2016; Accepted 2 August 2017

Journal of Cell Science (2017) 130, 3374-3387 doi:10.1242/jcs.200170

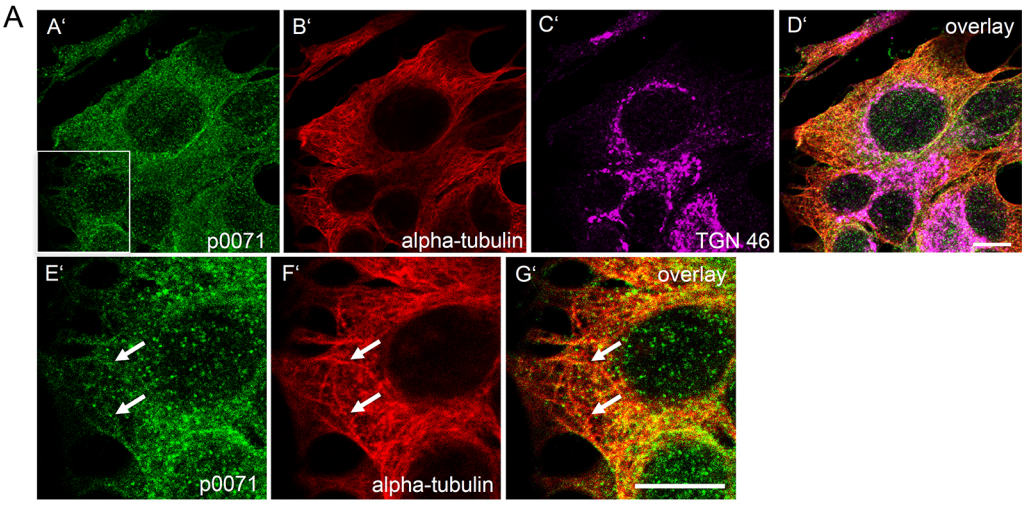

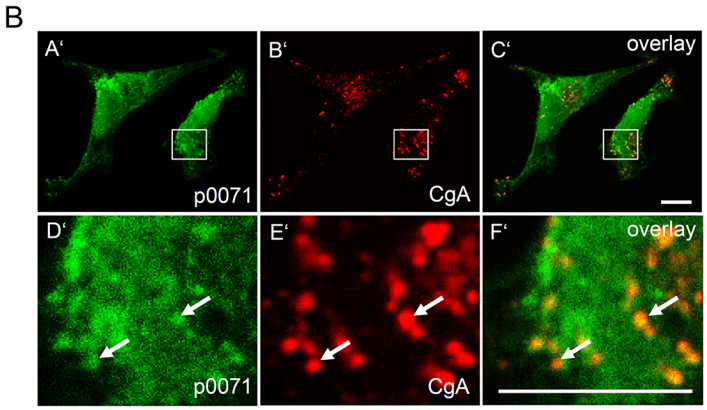

Fig. 1. Intracellular localization of p0071. (A) Confocal image sections of fixed BON cells stained for p0071 (green), α-tubulin (red) and the trans-Golgi network marker TGN46 (magenta). p0071 is observed at adhesion sites and throughout the cytoplasm, where it partially colocalized with microtubules (white arrows). (B) Partial colocalization of endogenous p0071 (green, FITC) with CgA-positive vesicular structures (red) in confocal image sections of BON cells (white arrows). Scale bars: 10 µm.

TGN46 (also known as TGOLN2), suggesting that p0071 is not involved in the control of vesicle biogenesis from the trans-Golgi network (TGN) (Fig. 1A).

The kinesin-2 microtubule motor protein KIF3B regulates the intracellular distribution of p0071 (Keil et al., 2009). Indeed, we observed a partial colocalization of p0071 with microtubules in the cytoplasm (Fig. 1A). Since peptide hormone-containing vesicles are transported along microtubules to their release sites (Elias et al., 2012), we examined whether p0071 would colocalize with CgA-positive vesicular structures. Interestingly, we observed a partial colocalization of p0071 with CgA granules in the cytoplasm, which was lost upon RNAi-mediated knockdown of p0071 (Fig. S1A), suggesting a potential role of p0071 in the intracellular transport of CgA-containing vesicles (Fig. 1B).

Knockdown of p0071 severely affects CgA release from BON cells

Thus, we next investigated whether p0071 depletion would impact on CgA intracellular transport in BON cells as measured by time-lapse microscopy with transiently transfected CgA-eGFP (Fig. 2A). Retention of CgA cargo at the TGN was induced at low temperature and transport reinitiated at 37°C. Control cells showed a depletion of the intracellular GFP signal corresponding to the secretion of CgA–eGFP into the supernatant within 25 min. In contrast, upon p0071 knockdown, CgA–eGFP was almost completely retained within the cell at the permissive temperature, suggesting a transport block. The intracellular retention of CgA–eGFP observed upon depletion of p0071 was similar to the phenotype observed following knockdown of protein kinase D2 (PKD2, also known as PRKD2), a Ca^{2+}/calmodulin kinase known to regulate release of CgA vesicles from the TGN (von Wichert et al., 2008) (Fig. 2A). The striking effects of p0071 depletion on CgA transport were confirmed by quantitative ELISA from BON culture supernatants (Fig. 2B). Knockdown of p0071 resulted in a significant reduction of CgA in BON supernatants that was again comparable to what was observed upon depletion of PKD2 (von Wichert et al., 2008) (Fig. 2B). To determine the specificity of p0071-mediated effects on CgA vesicle transport in BON cells, we performed rescue experiments by ectopically expressing p0071–HA following depletion of endogenous p0071 using an shRNA directed against the 3′UTR (shp0071 #1). Knockdown of p0071 significantly impaired CgA release, whereas re-expression of p0071 almost completely restored CgA secretion back to the level of controls (Fig. 2C).

Depletion of p0071 does not affect microtubule stabilization and polymerization

p0071 has been implicated in cytoskeletal organization (Hatzfeld and Nachtsheim, 1996; Keil et al., 2013; Wolf et al., 2006) and partially colocalized with microtubules in the cytoplasm of cells (Fig. 1A). Transmission electron microscopy revealed a marked intracellular accumulation of chromaffin vesicles in the cytoplasm of BON cells upon p0071 depletion (Fig. 2D). These data are in agreement with results obtained from our CgA–eGFP experiments (Fig. 2A–C). Moreover, the intracellular transport of CgA vesicles to

Journal of Cell Science (2017) 130, 3374-3387 doi:10.1242/jcs.200170

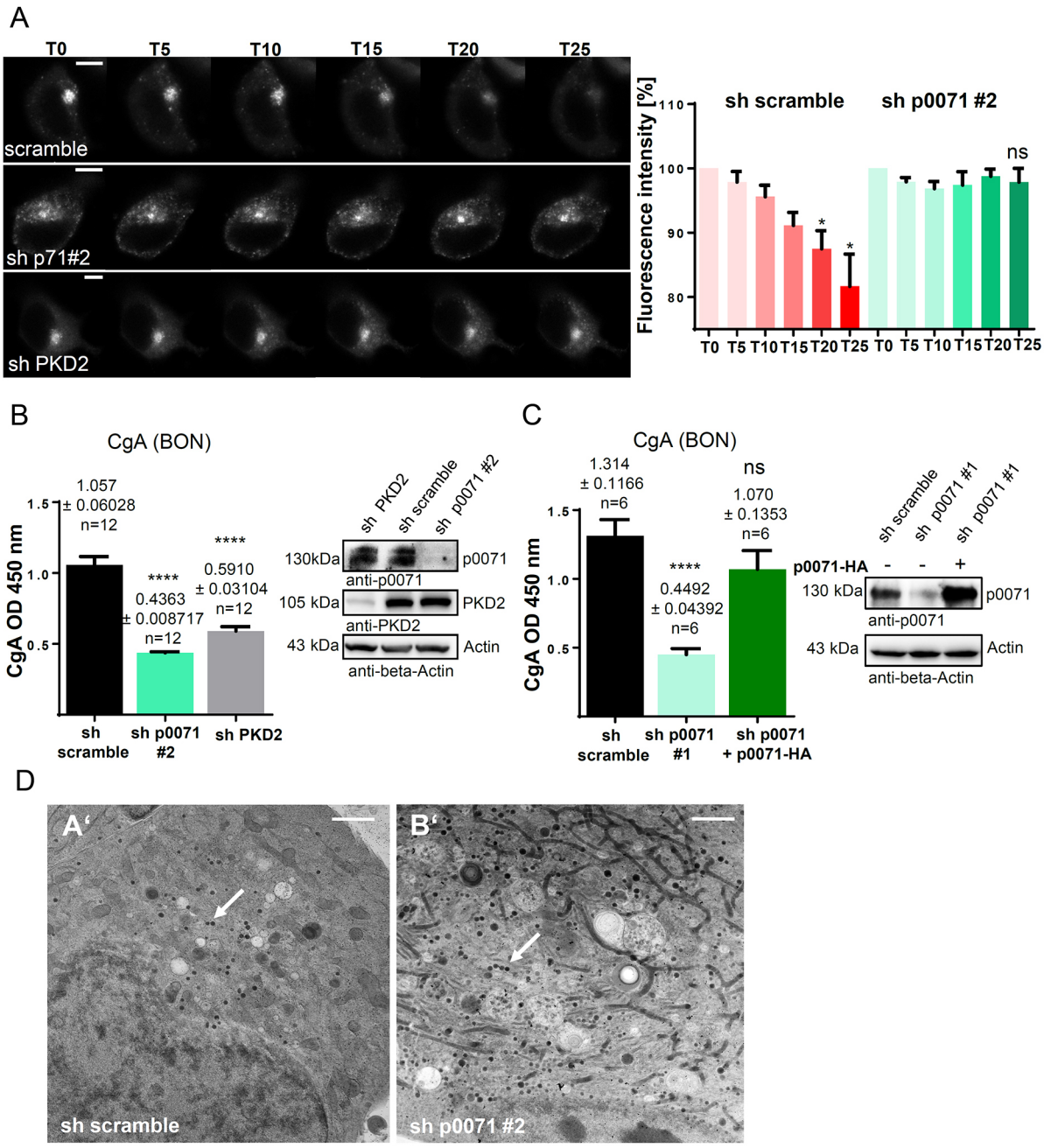

Fig. 2. Knockdown of p0071 severely impairs CgA secretion from BON cells. (A) Left-hand side, CgA–GFP video microscopy in BON cells. Images have been extracted from a live-cell video series showing intracellular fluorescence intensity of CgA–GFP after temperature-mediated block at the TGN and subsequent re-initiation of secretion over a time of 25 min. Cells with knockdown of p0071 showed intracellular retention in comparison to control cells. Right-hand side, statistical analysis of CgA–GFP fluorescence intensities in the analyzed cells (mean±s.e.m. from n=3 cells, each cell from an individual experiment). *P<0.05; ns, not significant (two-tailed unpaired Student's t-test). Cells with PKD2 knockdown to induce a block of secretion at the TGN were used as controls. Scale bars: 7.5 µm. T=time in minutes. (B) CgA ELISAs from BON cell culture supernatants. BON cells were lentivirally transduced to stably express shRNAs directed against p0071 or PKD2. CgA secretion by BON cells within 4 h was monitored. Graph, mean±s.e.m. of n=6 experiments in duplicate replicates. ****P<0.0001 (two-tailed unpaired Student's t-test). Right-hand panel, knockdown efficiency shown by western blotting. (C) Rescue of CgA secretion upon p0071 knockdown by ectopic expression of p0071. p0071–HA was transiently expressed in BON cells after depletion of endogenous p0071 by an shRNA targeting the 3′ UTR of the *p0071* mRNA. Scrambled shRNA was used as control. Graph, mean±s.e.m. of n=3 experiments with duplicate replicates. ****P<0.0001 (two-tailed unpaired Student's t-test). Right-hand side: western blots demonstrating expression levels of p0071 for an representative experiment. (D) Electron microscopy of BON cells treated with scrambled shRNA (left hand panel) and p0071-directed shRNA (right hand panel), respectively. Chromaffin secretory vesicles are visible as dark electron-dense rounded structures that have accumulated in p0071-knockdown cells (white arrows). Scale bars: 2 µm.

the plasma membrane along microtubules is affected by microtubule stability (Erickson, 1980; Joseph et al., 2008; Xie et al., 2010). Microtubule-targeting agents impair vesicle transport by affecting microtubule stability, and their long-term application causes microtubule network reorganization (Erickson, 1980; Thuret-Carnahan et al., 1985; Xie et al., 2010). We hypothesized that p0071 might influence CgA vesicle transport by modulating microtubules. Treatment of BON cells with the microtubule-

Journal of Cell Science (2017) 130, 3374-3387 doi:10.1242/jcs.200170

stabilizing drug taxol (Thuret-Carnahan et al., 1985) induced a perinuclear retention of CgA–eGFP as determined by time-lapse microscopy (Fig. S2A). Accordingly, CgA levels in culture supernatants as determined by ELISA assays were significantly reduced by taxol and also by the microtubule-depolymerizing agent vinblastine even at low concentrations (Fig. S2B). Thus, microtubule stability clearly impacts on intracellular cargo transport. Tubulin acetylation has been proposed as a marker for increased tubulin stability (Asthana et al., 2013; Webster and Borisy, 1989). We therefore tested whether p0071 would affect the stability of the microtubule network by assessing tubulin acetylation in the presence and absence of p0071 by using an acetylation-specific antibody. Taxol significantly enhanced microtubule acetylation and thus stability, in line with the literature (Erickson, 1980; Thuret-Carnahan et al., 1985; Xie et al., 2010), whereas knockdown of p0071 did not cause differences in tubulin acetylation (Fig. S2C). This suggests that p0071 does not regulate vesicle transport by modifying tubulin stability. Microtubules are polar structures that originate from microtubule-organizing centers (MTOCs) and constantly undergo a process of disassembly and regrowth. While their inward-bound ends (towards the MTOC) are referred to as minus-ends, the less stable outward oriented ends are termed plus-ends. End-binding protein 3 (EB3, also known as MAPRE3) binds to the plus-end of microtubules and stimulates microtubule growth (Akhmanova and Steinmetz, 2008). It is therefore used as a marker for microtubule polymerization. To investigate whether p0071 depletion would interfere with microtubule polymerization we employed mEOS–EB3 tracking microscopy (Fig. S2D; Movies 1 and 2). Tracking of EB3-positive plus-end comets in HeLa cells indicated no significant differences in polymerization rates upon p0071 depletion, whereas polymerization was significantly inhibited by taxol (Fig. S2D; Movies 1 and 2). Golgi membranes exist in an intimate relationship with microtubules, since microtubule stability and Golgi membranes influence each other (Chabin-Brion et al., 2001). To determine whether p0071 would interfere with microtubule-associated Golgi complex assembly, structure and maintenance, we performed nocodazole washout experiments. HeLa cells were either transduced with p0071-directed or scrambled shRNAs, and subsequently treated with nocodazole to depolymerize microtubules and induce Golgi dispersion. Subsequently, effects were reversed by nocodazole washout. Immunofluorescence analysis of the trans-Golgi marker TGN46 as well as α-tubulin indicated a strong dispersion of the Golgi complex and microtubule network at 2 h after addition of nocodazole (Fig. S2E). Following extensive washout, the Golgi complex and microtubule cytoskeleton reformation was completed after 2 h, regardless of the p0071 expression status (Fig. S2E). In summary, these data suggest that the regulation of cargo transport by p0071 appears to be independent of microtubule organization, polymerization and stability, and of structural changes at the Golgi compartment. Thus, the striking differences in CgA vesicle transport observed upon p0071 depletion are likely not directly dependent on the modulation of microtubule properties.

The kinesin-2 motor protein KIF3B is involved in the regulation of CgA transport

KIF3B forms a heterotrimeric motor complex together with KIF3A and the cargo adapter KAP3 (Verhey and Hammond, 2009). This complex transports proteins, including large dense core granules (Scholey, 2013), nucleic acids and organelles, towards the plus-ends of microtubules and the plasma membrane. KIF3B also directs intracellular positioning of p0071 (Keil et al., 2009) in a manner that is mediated through the interaction of the p0071-arm repeat domain with the C-terminus of KIF3B (Keil et al., 2009). We confirmed binding of p0071 to KIF3B by co-immunoprecipitation of p0071–HA and KIF3B–Flag proteins in HEK293T cells (Fig. 3A). Furthermore, endogenous KIF3B also colocalized with CgA-positive vesicles in BON cells (Fig. 3B), and this specific colocalization was lost upon shRNA-mediated KIF3B depletion (Fig. S1B). We next examined whether KIF3B was required for the transport of CgA-containing vesicles. Knockdown of KIF3B using two different shRNAs resulted in a marked reduction of CgA release from BON cells, which was comparable to the reduction observed upon p0071 depletion (Fig. 3C). Thus, p0071 and its interaction partner KIF3B, as a component of the KIF3 motor complex, are both involved in the transport of CgA vesicles.

p0071 depletion selectively affects secretion of cargos mediated by the KIF3 complex

Next, we asked whether p0071 has a general function in cargo transport mediated by the KIF3 complex. Therefore, we assessed whether p0071 would regulate other KIF3 cargos. Intracellular shuttling of matrix metalloprotease 9 (MMP9) is known to depend on KIF3 (Hanania et al., 2012). MMP9 is involved in extracellular matrix degradation as well as tumor angiogenesis, and thereby fulfills key functions in cancer cell invasion and metastasis (Egeblad and Werb, 2002; Wille et al., 2014). To explore a potential role of p0071 in MMP9 transport, we performed MMP9 ELISAs of culture supernatants from Panc1 pancreatic cancer cells (Fig. 4A). MMP9 levels in Panc1 cell supernatants were significantly reduced upon p0071 depletion. Effects were comparable to knockdown of PKD2, which blocks the shedding of MMP9-containing vesicles at the TGN and was used a respective control (Fig. 4A). To test whether p0071 would specifically regulate KIF3-dependent transport and not shuttling by other kinesin motors, we examined transport of vesicular stomatitis virus glycoprotein (VSV-G) vesicles, which is accomplished by kinesin-1 (Cai et al., 2009; Hirokawa et al., 2009; Kreitzer et al., 2000). Knockdown of p0071 did not interfere with VSV-G–eGFP transport in HeLa cells (Fig. 4B,C). In summary, transport of the KIF3 cargos CgA and MMP9 was impaired in different cell models (BON and Panc-1 cells) upon knockdown of p0071 whereas the transport by kinesin-1 was not affected. This suggests that p0071 plays a specific and vital role in anterograde microtubule transport mediated by the KIF3 motor complex.

p0071 depletion impairs directional movement of CgA vesicles along microtubules

In order to assess how p0071 might regulate KIF3-mediated CgA transport along microtubules, we tracked the movement of CgA–GFP-containing storage vesicles by time-lapse microscopy in BON cells (Fig. 5A–C; Movies 3 and 4). Both control and p0071-depleted cells exhibited spontaneous movement of vesicles in the cytosol after temperature-mediated cargo release from Golgi membranes (Fig. 5A,B; Fig. S3A). We also did not detect any changes in the overall velocity of CgA vesicles upon p0071 depletion (Fig. S3B). However, tracking of vesicles in the cytosol between the Golgi complex and the plasma membrane indicated significant deficiencies in directional vesicle movement upon p0071 knockdown. The Euclidean distance from the starting point to the end point of each track was significantly reduced by ∼50% in p0071-depleted cells compared to that in controls (Fig. 5A,B), pointing to a substantial loss of directional persistence (Fig. 5C). These effects could be demonstrated using two independent p0071-directed shRNAs (Fig. 5A–C). Again, depletion of the

Journal of Cell Science (2017) 130, 3374-3387 doi:10.1242/jcs.200170

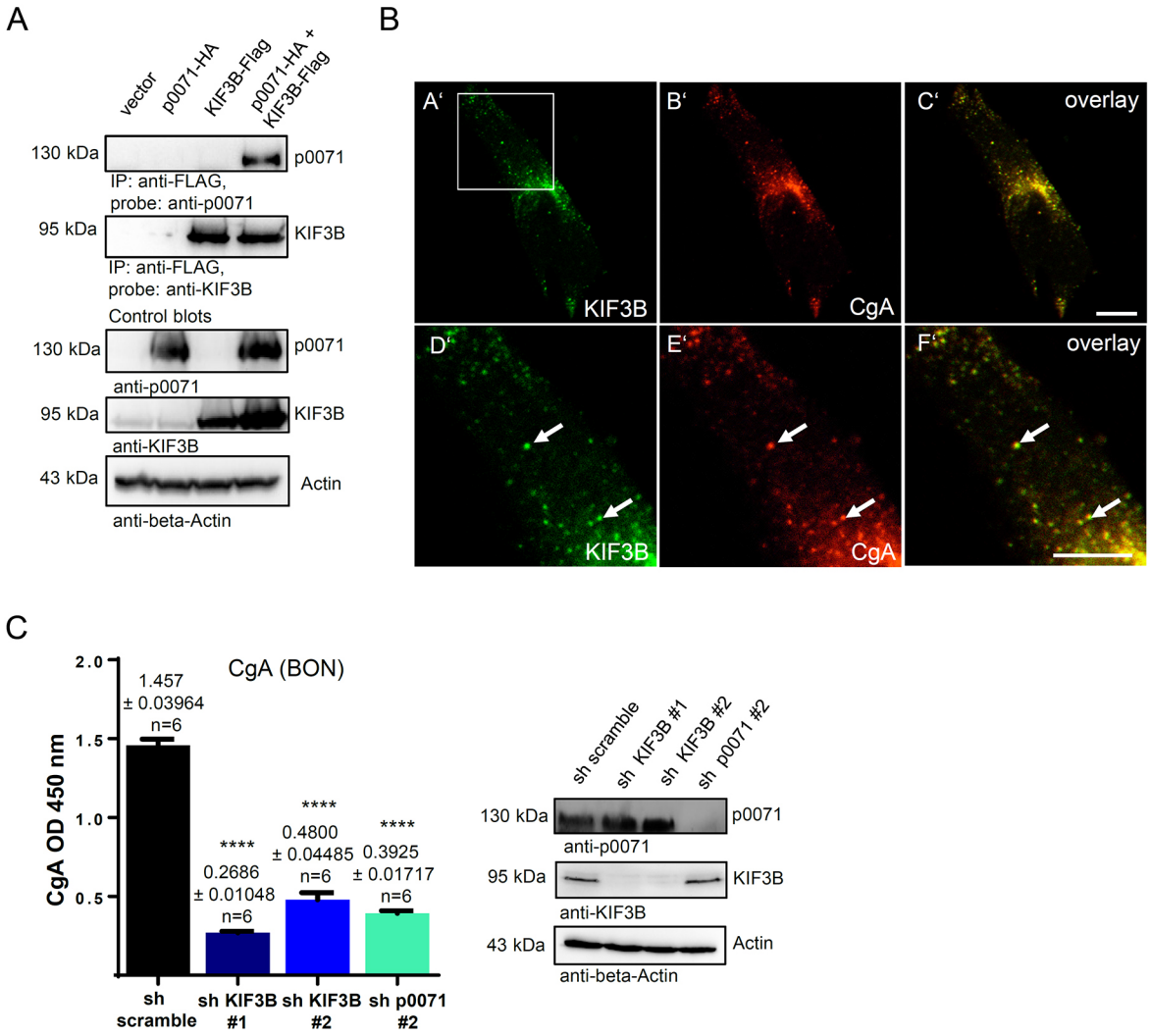

Fig. 3. KIF3B regulates CgA release from BON cells. (A) Co-immunoprecipitation experiment with ectopically expressed p0071–HA and KIF3B–Flag from HEK293T cell lysates. Flag-M2 antibody was used for immunoprecipitation (IP) and samples were probed using mouse monoclonal antibody against p0071 or rabbit polyclonal antibody against KIF3B, respectively. Protein expression in total cell lysates is shown in the lower panels referred to as 'control blots'. (B) KIF3B (green) colocalizes with CgA-positive vesicles (red) in BON cells (white arrows). A magnification of the indicated region is shown in the lower panels. Scale bars: 10 µm. (C) Left-hand side: statistical analysis of ELISA experiments (mean±s.e.m.) to quantify CgA in BON cell culture supernatants after 4 h of secretion following knockdown of KIF3B and p0071 via shRNAs. ****P<0.0001; ns, not significant (two-tailed unpaired Student's t-test). Right-hand side, western blot indicating protein expression levels in confluent cells used for ELISA experiments.

p0071-binding partner KIF3B (Keil et al., 2009) generated similar effects (Fig. 5A–C), suggesting a role of p0071 in the directional movement of CgA carriers transported by the KIF3 motor complex.

Kinesins constantly compete with dynein-mediated transport processes. This so-called 'tug-of-war' determines the directionality of vesicle movement (Gross et al., 2002; Soppina et al., 2009). Our data show, that upon p0071 knockdown directional persistence of KIF3-mediated transport is impaired. This results in an imbalance of transport processes so that they proceed at the same speed, but without a stringent direction towards the plasma membrane. At the molecular level, this phenotype may be caused by a change in the affinity of the kinesin motor domains towards microtubules, or by impairing the interaction of the KIF3 motor with cargo vesicles. In order to investigate the underlying molecular mechanisms, we performed quantitative acceptor-photobleach fluorescence resonance energy transfer (AB-FRET) analyses in BON cells to determine the relative proximity (binding) of the endogenous KIF3 complex (labeled with anti-KIF3B primary and Alexa Fluor 488 secondary antibodies) to microtubules stained by α-tubulin–mCherry. Our results indicated that FRET efficiencies for the interaction of KIF3B with microtubules were not significantly different between control and p0071-depleted cells (Fig. S3C), suggesting that p0071 does not modulate the KIF3B–microtubule association. In order to further verify these findings, we additionally performed *in vitro* microtubule-binding studies with KIF3B–FLAG that was affinity purified from lysates of scrambled shRNA-treated and p0071-depleted HEK293T cells (Fig. S3D–F). Indeed our *in vitro* experiments demonstrated that the amount of KIF3B–FLAG present in the 100,000 ***g*** microtubule pellet fractions was not significantly different for the respective conditions (Fig. S3D–F). This is in line with the literature indicating that p0071 does not directly interact with the motor domain of KIF3B (Keil et al., 2009).

p0071 interacts with the KIF3 complex protein KAP3

Since p0071 did not modulate the interaction of KIF3B with microtubules, it might regulate the interaction of the KIF3 motor

Journal of Cell Science (2017) 130, 3374-3387 doi:10.1242/jcs.200170

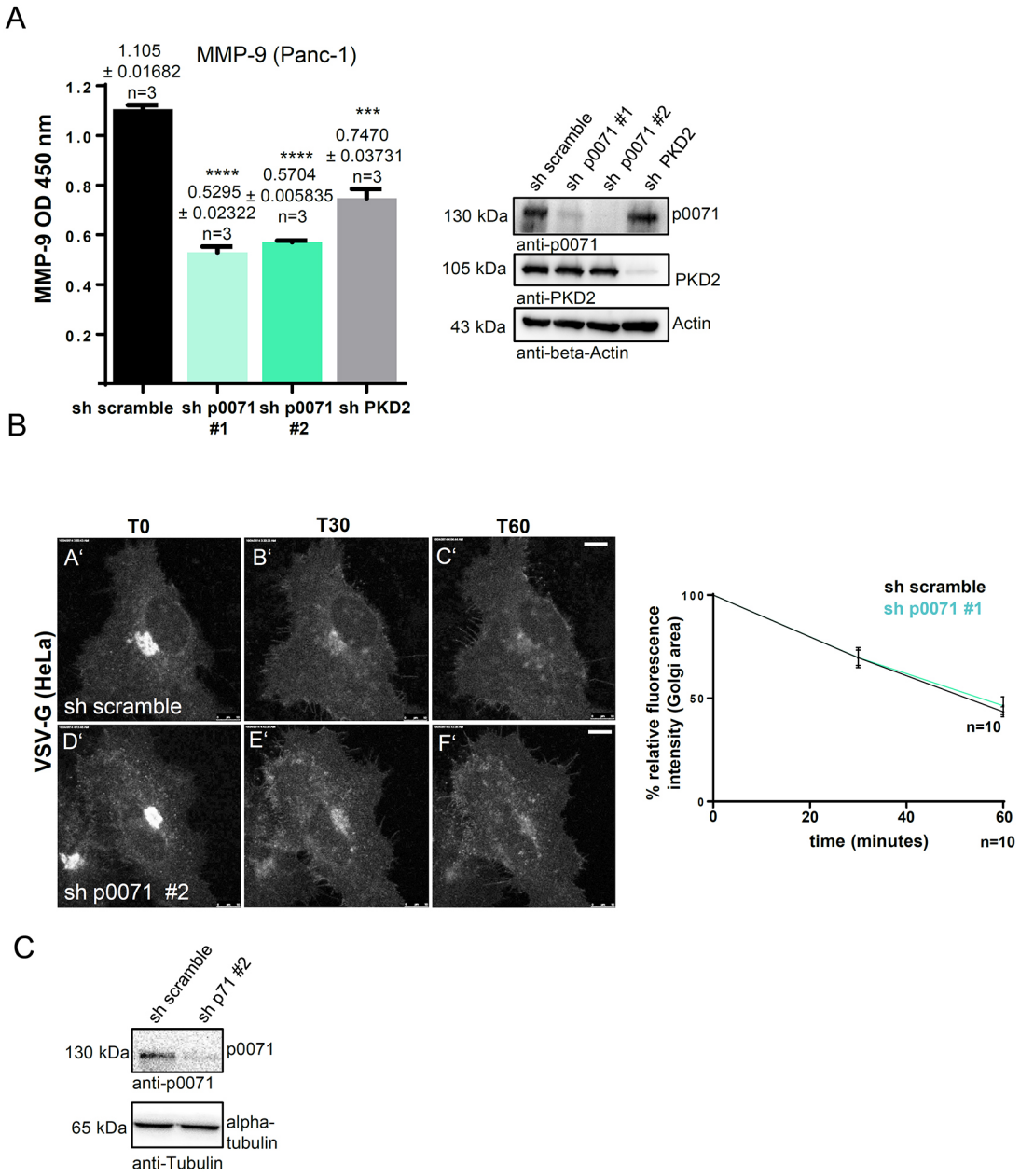

Fig. 4. p0071 selectively impairs transport of KIF3 cargos. (A) p0071 depletion impairs secretion of the KIF3 cargo MMP9. Left-hand side: secretion of MMP9 into cell culture supernatants of Panc1 cells. After 24 h, cell culture supernatants from p0071-knockdown cells (two different shRNA sequences) and scrambled shRNA controls were harvested and subjected to an ELISA assay. PKD2 knockdown, to block CgA release from the TGN, was used as control. Results are mean±s.e.m. ***P<0.001, ****P<0.0001 (two-tailed unpaired Student's t-test). Right-hand side, western blot of total cell lysates to confirm knockdown of proteins by shRNAs in Panc1 cells. (B) p0071 depletion does not affect kinesin-1-mediated VSV-G–GFP transport. AVSV-G–GFP transport assay were performed in HeLa cells transiently expressing VSV-G–GFP. Cells were cultured overnight at the non-permissive temperature for transport (39.5°C), followed by initiation of ER-to-Golgi transport (22°C, 2 h) and Golgi-to-plasma membrane transport (37°C) while protein synthesis was blocked by cycloheximide (20 µM). Left-hand side: intracellular VSV-G–GFP signal intensity was monitored for 1 h using a TCS SP8 confocal microscope. Right-hand side, fluorescence loss at the perinuclear area was quantified by measuring signal intensities over time within an ROI drawn around the Golgi area in registered images using ImageJ. Mean±s.e.m. from n=10 cells; results were not significant (two-tailed unpaired Student's t-test). (C) Detection of p0071 knockdown by western blotting lysates from HeLa cells as used in experiments.

with the cargo vesicles. The heterotrimeric KIF3 complex comprises of the motor units KIF3A and KIF3B as well as the associated protein KAP3 (KIFAP3) (Doodhi et al., 2009; Kondo et al., 1994; Scholey, 2013; Takeda et al., 2000; Yamazaki et al., 1995, 1996). Many functions for KAP3 are still elusive, but it has been suggested to be required for effective cargo binding (Doodhi et al., 2009; Scholey, 2013). KAP3 also interacts with cargo molecules, such as fodrin, APC (Jimbo et al., 2002; Takeda et al., 2000) or dynactin in melanosomes (Deacon et al., 2003). We therefore tested whether depletion of KAP3 would also affect secretion, similar to results obtained upon knockdown of KIF3B and p0071 (Figs 2B and 3C). In line with that data, knockdown of KAP3 also significantly impaired secretion of CgA from BON cells (Fig. 5D). We next explored whether p0071 was involved in the KIF3–KAP3

Journal of Cell Science (2017) 130, 3374-3387 doi:10.1242/jcs.200170

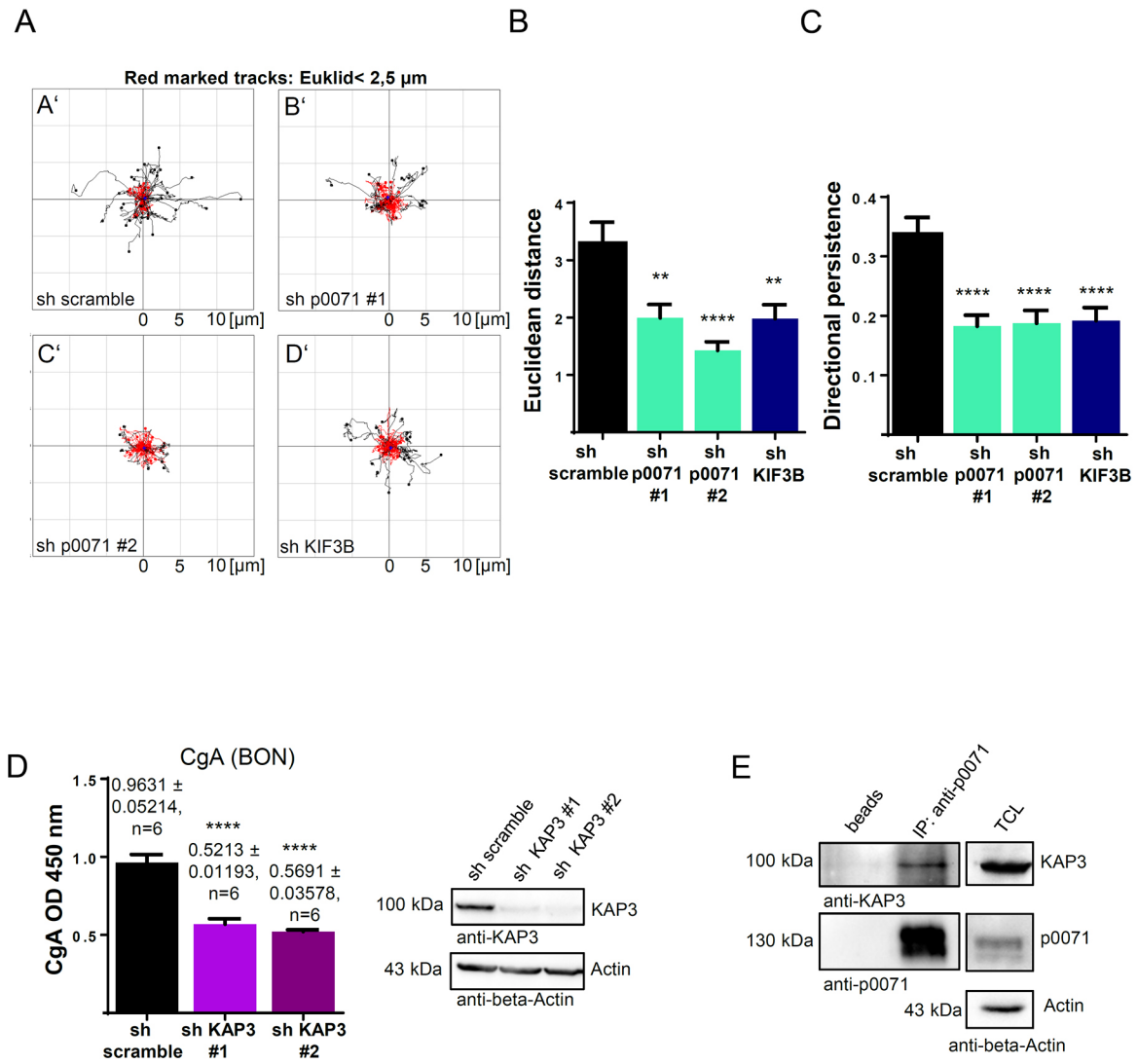

Fig. 5. p0071 controls directional persistence of KIF3 cargo vesicle movement and interacts with KAP3. (A) Visualization of Euclidean distance traveled by CgA–GFP vesicles in BON cells tracked via live-cell imaging. The center of graphs represents track starting points and tracks exceeding an Euclidean distance between start and end point of 2.5 µm are presented in black, while tracks showing little directional persistence and a Euclidean distance shorter than 2.5 µm are shown in red. Tracking was carried out for varying time intervals dependent on the disposition of vesicles in the microscope focus layer. Analyses of forty tracks per condition are shown. (A′) Euclidean distance for control cells. (B′) Euclidean distance for p0071 knockdown shRNA #1. (C′) Euclidean distance for *p0071* knockdown shRNA #2. (D′) Euclidean distance for KIF3B knockdown. (B) Statistical analysis (mean±s.e.m.) of Euclidean distance for CgA–GFP vesicles in BON cells. 40 tracks per condition (control shRNA; shp0071 # 1&2; shKif3B, see also A) were quantified. ***P*<0.01; *****P*<0.0001 (two-tailed unpaired Student's *t*-test). (C) Statistical analysis (mean±s.e.m.) of directional persistence for CgA–GFP vesicle tracks shown in A, calculated from values for Euclidean divided by accumulated distances of each track. *****P*<0.0001 (two-tailed unpaired Student's *t*-test). (D) Left-hand side, CgA ELISA from BON cell culture supernatant. Cells were treated with scrambled shRNA and two different shRNAs targeting KAP3. Results are mean±s.e.m. *****P*<0.0001; ns, not significant (two-tailed unpaired Student's *t*-test). Right-hand side: western blot indicating protein expression levels for cells used in experiments. (E) Co-immunoprecipitation of endogenous p0071 and KAP3 from BON total cell lysate. Guinea pig polyclonal anti-p0071 antibody was used for immunoprecipitation (IP) and monoclonal anti-KAP3 as well as anti-p0071 antibodies were used for probing samples. As a negative control, the cell lysate was incubated with empty beads (left lane of left hand panel). Right-hand panel, expression of respective proteins and knockdown controls in total cell lysate (TCL).

interaction. First, we examined whether p0071 would bind to KAP3 by co-immunoprecipitation experiments for endogenous proteins from BON lysates (Fig. 5E). Indeed, we were able to show endogenous KAP3 in p0071 immunoprecipitates (Fig. 5E). This interaction was further confirmed by AB-FRET experiments demonstrating a significant increase in the fluorescence donor signals of p0071 stained with p0071 primary and Alexa-Fluor-488-conjugated secondary antibodies (donor molecule) after depletion of the acceptor KAP3–V5–His marked by anti-V5 primary and Alexa-Fluor-568-conjugated secondary antibodies (Figs S3G,I and S4A) at CgA-positive structures (marked with Alexa Fluor 647). In contrast, we could not detect a direct interaction of CgA marked with anti-CgA primary and Alexa Fluor 647 secondary antibodies, packaged in granules, with the cargo adaptor KAP3–V5–His stained with anti-V5 primary and Alexa Fluor 568 secondary antibodies in corresponding FRET experiments (Fig. S3H,I). In order to map the interaction of p0071 with KAP3, we performed GST-pulldown experiments using bacterially purified p0071-head, p0071-armadillo-repeat and p0071-tail domains (Fig. 6A,B). KAP3–V5–His was expressed in HEK293T cells, and was only pulled down

Journal of Cell Science (2017) 130, 3374-3387 doi:10.1242/jcs.200170

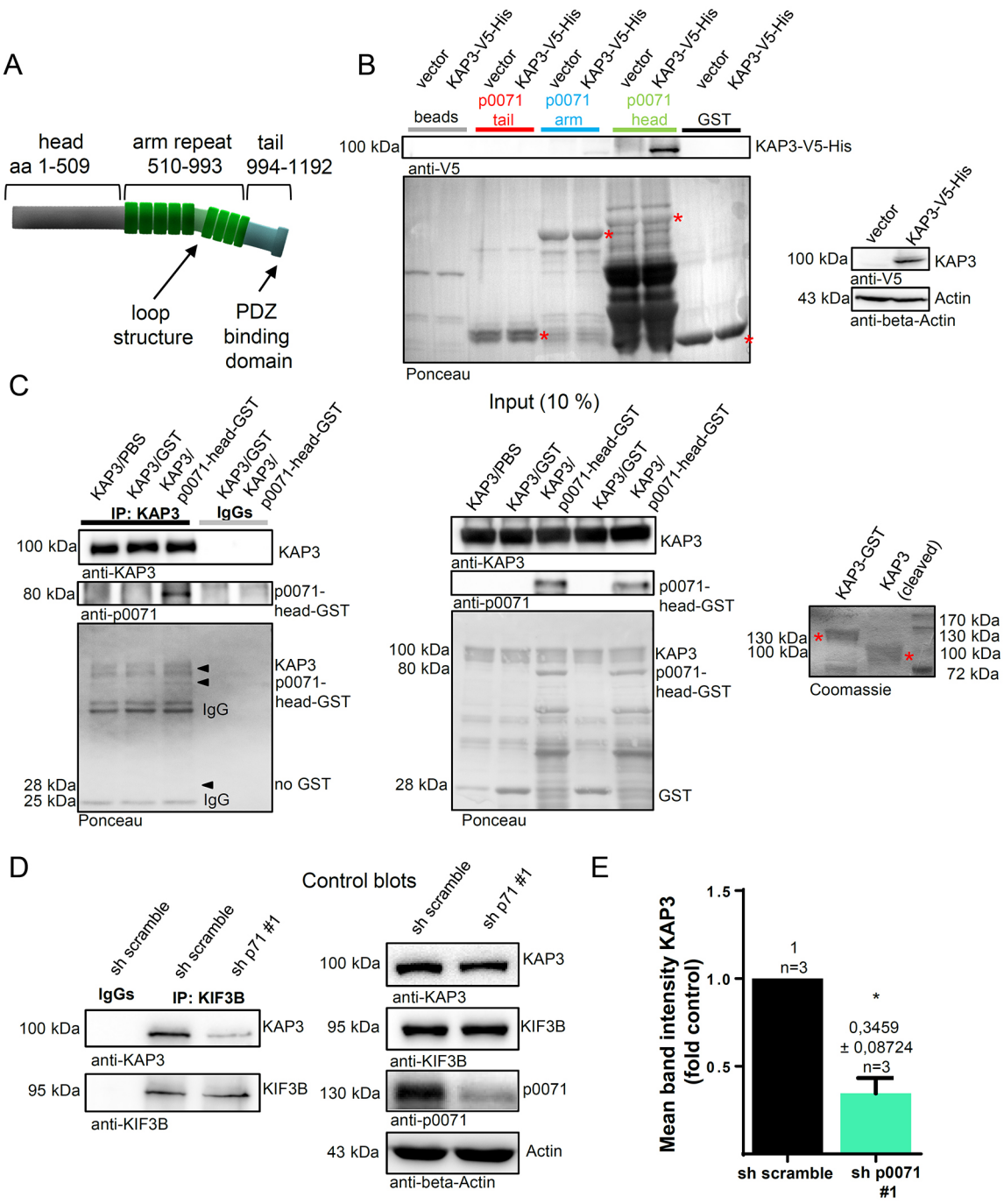

Fig. 6. p0071 interacts with KAP3 via its large head domain. (A) Schematic illustration of the three domains of p0071. Respective amino acid residues are indicated. (B) Left-hand panel, pulldown experiment to demonstrate specific binding of KAP3 to individual domains of p0071. KAP3–V5–His was expressed in HEK293T cells and cell lysate was incubated with purified GST–p0071-head, GST–p0071-arm repeat and GST–p0071 tail domains immobilized on GST–sepharose beads, respectively. GST-loaded beads as well as cells transfected with empty vector were used as negative controls in each experiment. Ponceau staining of the respective membrane shows the presence of GST proteins. Asterisks mark the full-length GST proteins. Right-hand panel, expression of KAP3–V5–His in HEK293T cells. (C) *In vitro* binding study of the p0071-head domain with KAP3. p0071-head–GST and KAP3 (GST-tag cleaved) were bacterially expressed and purified, and then incubated overnight and immunoprecipitated (IP) with anti-KAP3 antibody as well as Protein-A–Sepharose beads (left-hand side). Middle panel, purified proteins detected in the input samples by western blotting and Ponceau staining of respective membranes. Bound p0071-head was detected by western blotting. Lower panels show Ponceau staining of the membrane indicating that GST alone does not bind to KAP3 and position of indicated proteins (arrowheads). Right-hand side, Coomassie-stained SDS gel with purified KAP3–GST before (left-hand lane in gel) and after (right-hand lane) removal of the GST tag by HRV3C protease. A shift in the molecular mass is clearly visible (asterisks). (D) Left-hand side: co-immunoprecipitation experiment of KIF3B and KAP3 from BON cell lysates following treatment with control shRNA or shp0071 #1. Right-hand side, expression of respective proteins and knockdown controls in total cell lysates. Rabbit polyclonal anti-KIF3B was used for immunoprecipitation (IP) and mouse monoclonal anti-KAP3 or rabbit polyclonal anti-KIF3B antibodies were used for probing immunoprecipitates, respectively. (E) KAP3 signal intensities were normalized to the dedicated intensity of KIF3B immunoprecipitate bands. Statistical analysis (mean±s.e.m.) of co-precipitated KAP3 in KIF3B IPs; n=3 experiments. *P<0.05 (two-tailed paired Student's t-test).

Journal of Cell Science (2017) 130, 3374-3387 doi:10.1242/jcs.200170

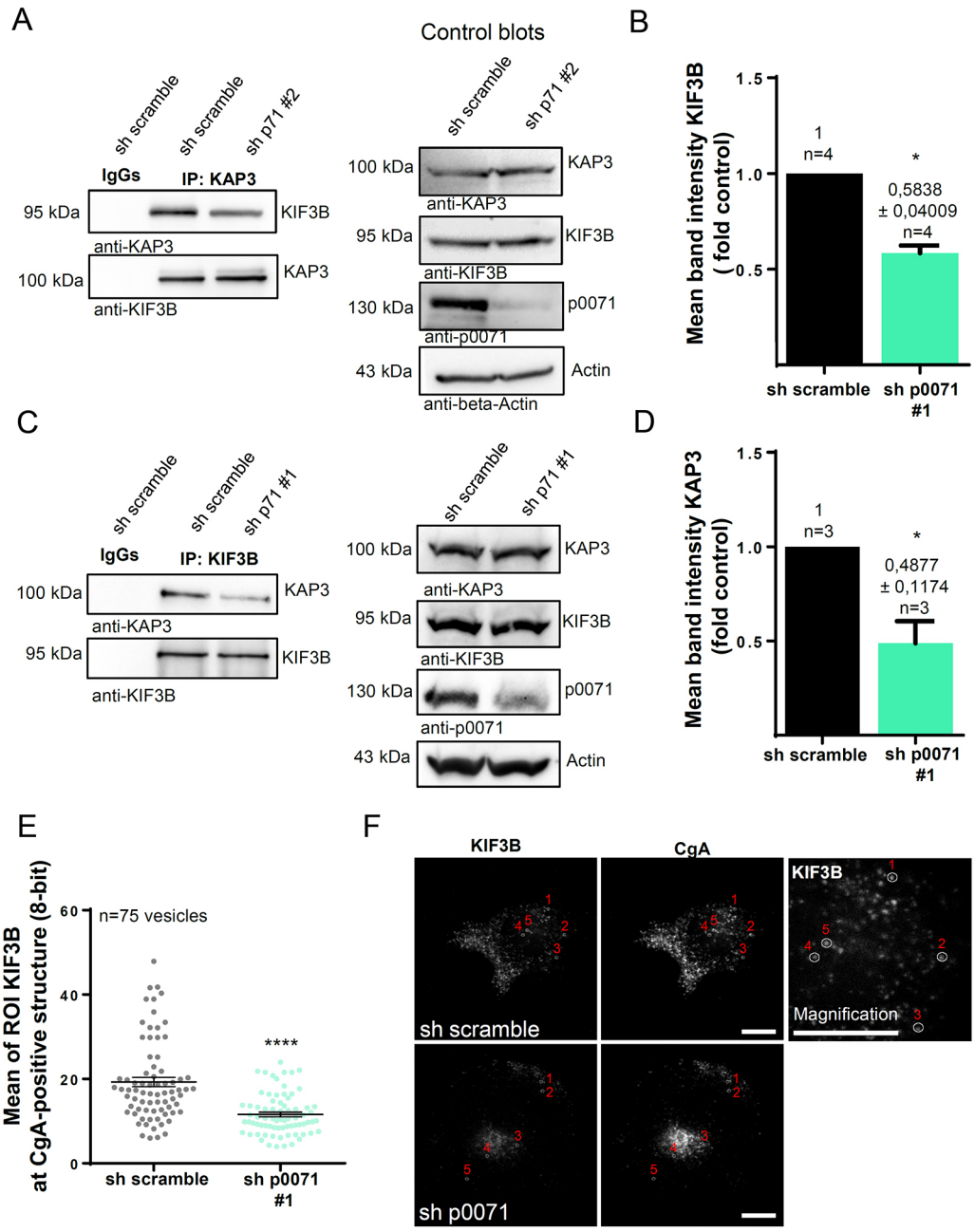

Fig. 7. p0071 stabilizes binding of KAP3 to KIF3B within the KIF3 complex. (A) Co-immunoprecipitation experiment as in Fig. 6D using KAP3 antibody for immunoprecipitation (IP). (B) Quantification of four experiments as shown in A; KIF3B band intensities were normalized to KAP3 IP bands. Results are mean±s.e.m. *P<0.05 (two-tailed paired Student's t-test). (C) Co-immunoprecipitation experiment of KIF3B and KAP3 in Panc1 cells performed as shown in A. (D) Statistical analysis of three independent KIF3B– KAP3 co-immunoprecipitation experiments shown in C. KAP3 band intensities were normalized to KIF3B IP bands. The graph shows mean±s.e.m. of co-precipitated KAP3. *P<0.05 (two-tailed paired Student's t-test). (E) BON cells were treated with scrambled shRNA and p0071-directed shRNA (shp0071 #1), respectively and transfected to express α-tubulin–mCherry to visualize microtubules. KIF3B and CgA were stained with specific primary and secondary antibodies. Signal intensities in sub-ROIs around single peripheral CgA vesicles were measured and quantified from confocal image sections recorded with equal settings for the KIF3B–Alexa-Fluor-488 channel. The graph depicts mean±s.e.m. of 15 cells with five sub-ROIs (single CgA vesicles) per cell. ****P<0.0001 (two-tailed unpaired Student's t-test). (F) Representative images showing sub-ROIs at vesicular structures in a control cell and a p0071-knockdown cell, respectively, for the experiment quantified in E. Scale bars: 10 µm.

from lysates by the p0071 head, but not the p0071 armadillo or tail, domains (Fig. 6B). We confirmed the specificity of our pulldown experiments by investigating the binding of p0071 domains to the KAP3 cargo MMP9–GFP. As cargo stored in vesicles, MMP9–GFP should not directly bind to p0071. In line with this assumption, we did not detect any signal in our pulldown experiments (Fig. S4B). To additionally verify a direct interaction between KAP3 and p0071, we performed *in vitro* binding experiments using purified bacterially expressed KAP3 and p0071-head–GST proteins (Fig. 6C). Indeed, we were able to show that both proteins directly bind to each other. Subsequently, we analyzed whether depletion of p0071 would affect the interaction of KIF3B and KAP3. Interestingly, knockdown of

Journal of Cell Science (2017) 130, 3374-3387 doi:10.1242/jcs.200170

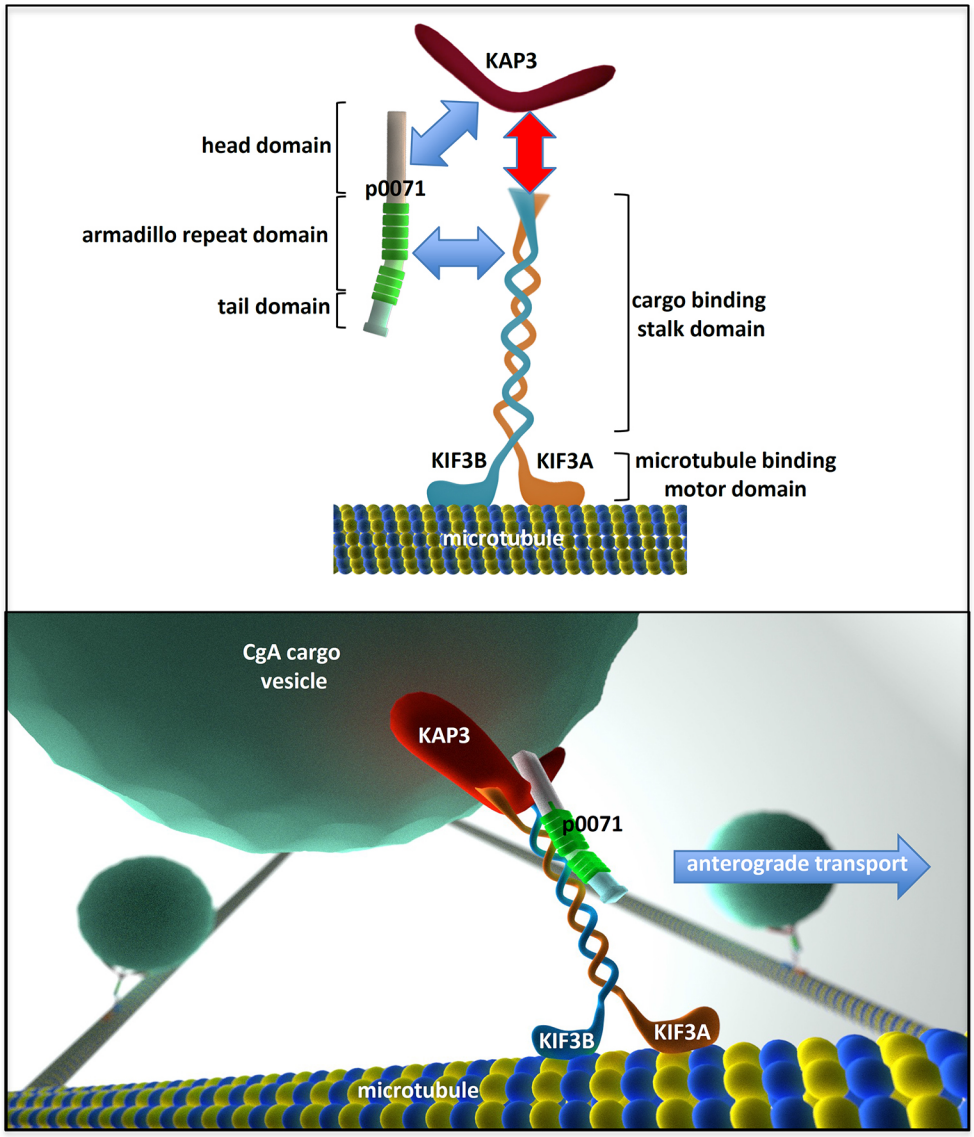

Fig. 8. Schematic illustration of the molecular interactions of p0071 with the heterotrimeric KIF3 motor complex. KIF3A and KIF3B are shown in orange and blue, respectively, and indirectly bind to the cargo vesicle (dark green in lower panel) via the cargo adaptor protein KAP3 (red). The p0071 armadillo domain (bright green) binds KIF3B whereas its head domain (gray) binds to KAP3 thereby stabilizing the kinesin complex to facilitate cargo association and transport. Interaction of individual p0071 subdomains with KAP3 and KIF3B, respectively, are indicated by blue double arrows, and binding of the KIF3 motor subunits to KAP3 is depicted by the red double arrow.

p0071 with two specific shRNAs significantly impaired the interaction of KIF3B and KAP3 in BON cells. Co-immunoprecipitation experiments demonstrated that, upon p0071 depletion, the amount of KAP3 associated with KIF3B and, vice versa, the portion of KIF3B detected in KAP3 immunoprecipitates was significantly less with respect to cells treated with control shRNA (Figs 6D,E and 7A,B; Fig. S4C–E). These results were confirmed in Panc1 cells (Fig. 7C,D), that were used to study KIF3-mediated MMP9 secretion in Fig. 4B (Hanania et al., 2012; Wille et al., 2014). Again, depletion of p0071 significantly impaired the interaction of KIF3B and KAP3 as indicated by a markedly weaker co-immunoprecipitation of KAP with KIF3B (Fig. 7C,D), suggesting that p0071 functions as a linker to stabilize the KIF3–KAP3 complex. In order to further explore such a stabilization at cargo vesicles, we quantified KIF3B signal intensities at CgA-positive structures in the cytoplasm of BON cells (Fig. 7E,F; Fig. S4F). Indeed, depletion of p0071 resulted in a significant loss of KIF3B signal at CgA-positive vesicles with respect to that of control cells (Fig. 7E,F). In summary, these data indicate that p0071 fosters the interaction of the KIF3B and KAP3 subunits of the KIF3 motor complex thereby regulating directional transport of KIF3 cargos.

DISCUSSION

In this study, we describe an entirely new regulatory function of the p120-catenin family protein p0071 in intracellular transport of CgA in neuroendocrine tumor cells and of MMP9 cargo in Panc-1 cells. Transport of both cargos was severely impaired upon p0071 knockdown (Figs 2 and 4A). This was surprising, since p0071 had not been previously implicated in cargo transport and the secretory pathway. Our data indicate that the microtubule cytoskeleton has a vital function in p0071-regulated intracellular vesicle transport (Figs 1A and 5, Figs S2 and S1A). However, p0071 did not affect microtubule stability, polymerization or Golgi organization (Figs S2A–E; Movies 1 and 2). Transport of dense core granules and of MMP9 to the plasma membrane depends at least partially on the KIF3 motor complex (Hanania et al., 2012; Hirokawa et al., 2009). Depletion of the KIF3B motor subunit resulted in a similar transport phenotype to that seen upon p0071 knockdown (Figs 3C and 5). p0071 can directly interact with KIF3B (Keil et al., 2009, 2013). Since knockdown of p0071 had no effect on cargo transport to the plasma membrane mediated by other microtubule motors, such as kinesin-1 (Fig. 4B), p0071 seems to be specifically required for the transport of cargo shuttled to the plasma membrane by KIF3 motors.

Journal of Cell Science (2017) 130, 3374-3387 doi:10.1242/jcs.200170

The heterotrimeric KIF3 motor complex comprises the KIF3A and KIF3B motor subunits as well as the associated protein KAP3, which was suggested to serve as a tightly bound adaptor for cargo binding (Scholey, 2013). KIF3 motors mediate plus-end-directed anterograde transport towards the plasma membrane. Transport in the reverse, minus-end, direction is processed by dynein. Activities of these opposing microtubule motors then produce bidirectional movement of cargo vesicles (De Rossi et al., 2015; Deacon et al., 2003; Fu and Holzbaur, 2013; Gross et al., 2002; Scholey, 2013). Two models have been postulated to explain these processes. In the 'coordination model' distinct mechanisms are proposed that switch different sets of motors on or off (Fu and Holzbaur, 2013; Gross et al., 2002). In the 'tug-of-war' model a competition between opposed polarity motors is postulated (Blehm and Selvin, 2014; Hendricks et al., 2010; Soppina et al., 2009). Here, the 'stronger team' wins the competition and defines the direction of the cargo. It is currently accepted that there is a complex interplay between local tug-of-war interactions on the cargo vesicles and larger regulatory events that bias the outcome of the tug-of-war (De Rossi et al., 2015). Our data fit both models. Analysis of CgA cargo vesicle movement along microtubules revealed that p0071 is required for the directional persistence of vesicle transport, since in the absence of p0071 vesicles moved erratically (Fig. 5A–C; Movies 3 and 4), whereas their overall velocity was unchanged (Fig. S3B). p0071 interacts with the KIF3B motor protein via its armadillo repeats (Keil et al., 2009). We identified a novel interaction of p0071 with KAP3 via the p0071 head domain (Figs 5E and 6A–C). The presence of p0071 stabilized the interaction of the KIF3B motor subunit with the cargo-binding protein KAP3 (Figs 6D,E and 7A–D; Fig. S4C–E). If KIF3 motors are not properly loaded with cargo or the affinity of cargo binding is reduced (Hill et al., 2004; Luby-Phelps et al., 1987), KIF3-transported carriers could easily lose the local tug-of-war and move with dyneins towards microtubule minus-ends. On the other hand, the presence of p0071 might also act as an activating switch that allows for proper activation of the KIF3 motor complex by fostering an interaction within the heterotrimeric complex. In this context, it was recently shown that intermolecular communication within the KIF3A–KIF3B heterodimer modulates entry into the processive run of motors (Albracht et al., 2016). Recent models also suggest that one kinesin, but multiple dyneins, are associated with a cargo vesicle (De Rossi et al., 2015). Interestingly, dyneins are able to 'step backwards' into the direction of kinesin motors, whereas kinesins cannot do the same [e.g. during melanosome transport kinesin-2 is suggested to temporarily detach from microtubules but stays connected to the cargo carrier during dynein-favored movement (De Rossi et al., 2015)]. Our finding may be part of an alternate molecular mechanism that might help to control these competing processes. If the interaction between KIF3B and KAP3 is lost, we also lose directional persistence during movement of cargo (Fig. 5A–C). We show that depletion of p0071 results in a weakened KAP3–KIF3B binding (Figs 6D,E and 7A–D; Fig. S4C–E), while the interaction of the KIF3 motor subunit with the microtubules remains intact, as demonstrated by FRET interaction studies and *in vitro* microtubule binding assays (Fig. S3C–F). In addition, we show that depletion of p0071 also results in impaired KIF3B signals quantified at CgA-positive vesicular structures (Fig. 7E,F; Fig. S4F). Our data therefore suggest a mechanism by which the motor more readily detaches from the cargo vesicle in the absence of p0071, which also might explain the observed loss of directional persistence during plasma membrane-directed transport.

In conclusion, the data presented in this study suggest the following model (Fig. 8). The p120-catenin family protein p0071 binds to the microtubule motor subunit KIF3B with its armadillo repeats and interacts with the associated cargo-binding protein KAP3 via its head domain, thereby stabilizing the interaction of KIF3B and KAP3. If p0071 is lost from the complex, there is a strongly aberrant movement of KIF3–motor cargos, indicated by a significant reduction in directional persistence of CgA vesicles on microtubules transported towards the plasma membrane. This ultimately results in impaired secretion of the KIF3 cargos CgA or MMP9 from BON and Panc1 cells, respectively.

p0071 therefore is a novel and crucial partner in the molecular regulation of transport processes that depend on the KIF3 motor complex. Our data are compatible with, and expand the current models that try to integrate the regulation of plus- and minus-end-directed transport by dyneins and kinesins. This is accomplished through an additional regulatory function of p0071 stabilizing the interaction of the heterotrimeric KIF3 motor complex with cargo vesicles.

MATERIALS AND METHODS

Cell culture and transfection

Human BON (authenticated in February 2014; Münzberg et al., 2015) and Panc1 (freshly purchased from the European Collection of Cell Cultures through Sigma-Aldrich, St Louis, MO) pancreatic tumor cell lines, and HeLa cells were maintained in Dulbecco's modified Eagle's medium (DMEM) supplemented with 10% (v/v) fetal bovine serum in a humidified atmosphere of 5% CO_2:95% air at 37°C. Transfection of BON and HEK293T cells was performed using PEI (Polysciences Inc., Warminster, PA). HeLa cells were transfected with HeLa Monster reagent (Mirus Bio, Madison, WI). Panc1 cells were transfected using FuGENE HD (Promega, Madison, WI) according to the manufacturer's instructions. Stable cell lines were generated by lentiviral transduction and selected using 6 µg/ml puromycin. For virus production, HEK293FT cells were transfected with lentiviral expression and packaging constructs as described previously (Sroka et al., 2016). Virus containing supernatants were harvested after 48 h and used for transduction of BON, HeLa and Panc1 cells, respectively.

Plasmids and RNA interference

The pVen2-HA-p0071(wt) and pcDNA3-KIF3B-wt-Flag eukaryote expression plasmids as well as the bacterial expression vector p0071-R (510-993)-pGex5 were described previously (Keil et al., 2009). P71-head (1-509)-pGex5.1 and p0071(tail)-pGex-5X-1 were generated by cloning the p0071 head domain (amino acids 1–509) into pGEX5.1 using the MunI and EcoRI restriction site and the tail domain (amino acids 994–1149) into pGEX-5X-1 using the EcoRI and XhoI restriction sites, respectively. The plasmid pEF-DEST51-KAP3-V5-His was acquired from Source bioscience (Nottingham, UK). For bacterial protein expression of KAP3, the gene sequence was cloned into pGEX-6P3 using EcoRI and Xho1 restriction sites introduced by the following oligonucleotides: 5′-GCTAT-GAATTCGCAAGGGGAGGACGCCAGATACCTC-3′ as forward primer and 5′-ATTCTCGAGTCAAGATCCATAGCCATAG-3′ as reverse primer, respectively. The pcDNA3-tubulin-mCherry and mEOS-EB3 expression vectors were a kind donation from Prof. Franz Oswald (Ulm University, Ulm, Germany). The CgA–GFP expression construct has been described in von Wichert et al. (2008). p0071- and KIF3B-specific shRNA constructs were purchased from Thermo Scientific (GE Dharmacon, Lafayette, CO). Two p0071 hairpins, one directed against p0071 3′ UTR (TRCN0000123179, referred to in text as shp0071 #1 in experiments) and one directed against p0071 cDNA (TRCN0000123181, referred to as shp0071 #2) were selected for experiments. Two KIF3B-specific shRNAs (TRCN0000116458, referred to as shKIF3B #1 and TRCN0000116460, referred to as shKIF3B #2) were used for the experiments. Constructs used to generate KAP3 knockdown cell lines as follows: clone IDs TRCN0000117237 (referred to as shKAP3 #1) and TRCN0000117238 (referred to as shKAP3 #2). The PKD2 shRNA (NM_016457.x-294s1c1]) was obtained from Sigma-Aldrich, St Louis, MO.

Journal of Cell Science (2017) 130, 3374-3387 doi:10.1242/jcs.200170

Treatment of cells with microtubule-targeting agents

Unless otherwise indicated, cells were serum starved and treated with 10 nM paclitaxel (taxol) (Sigma-Aldrich) or 5 nM vinblastine (Sigma-Aldrich), respectively. CgA secretion assays were carried out after 16 h of incubation. Tubulin acetylation was assessed by western blotting from total cell lysates after incubation times of up to 72 h. For nocodazole treatment, cells were incubated with 2.5 µg/ml nocodazole (Sigma-Aldrich) for 2 h at 37°C. Washout was achieved by rinsing five times and transferring to fresh medium for 2 h before fixation.

Immunofluorescence microscopy

BON and HeLa cells were seeded on glass coverslips, and after 24 h (unless indicated otherwise) fixed and permeabilized with cold methanol for 5 min. Samples were blocked and stained in PBS containing 5% fetal bovine serum (FBS) and 0.05% Tween-20. Primary and secondary Alexa Fluor-conjugated (Invitrogen, Carlsbad, CA, USA) antibodies were added for 2 h at room temperature followed by washing samples with PBS five times for 5 min. Coverslips were mounted using Fluoromount-G (Southern Biotech, Birmingham, AL). Primary antibodies used for immunofluorescence staining include antibodies against p0071, KIF3B, KAP3, α-tubulin, TGN46 and anti-chromogranin A. A full list of primary and secondary antibodies used for immunofluorescence including dilution, catalog numbers, vendors and literature references is available in Table S1. Signal intensities were measured by quantifying the mean of the region of interest (ROI) intensities within a defined sub-ROI using the ImageJ software (Schneider et al., 2012), and statistical analysis was performed using Prism 6.0 (GraphPad, San Diego, CA). AB-FRET experiments were performed and quantified as described previously (Eiseler et al., 2016; Sroka et al., 2016; Wille et al., 2014). In brief, pre-bleach and post-bleach images of donor and acceptor were acquired in an automated time series. Acceptor bleaching was performed using an intensive 561-nm laser line in a defined region of interest as representatively shown in Fig. S3. Single percentage FRET values, as well as mean FRET efficiency and s.e.m. of non-thresholded raw data were calculated, and statistical significance was determined by using a two-tailed unpaired Student's *t*-test.

Live-cell video and confocal imaging

For live-cell imaging, cells were seeded onto 35 mm microscopy dishes (ibidi GmbH, Martinsried, Germany) 24 h prior to treatment. For nocodazole washout experiments and microtubule end point tracking, an inverted Olympus IX71 microscope (Olympus, Hamburg, Germany) equipped with an ORCA R2 camera (Hamamatsu Orca, Hamamatsu, Japan) and Simple PCI Software (Compix, Irvine, CA) was utilized. For all other experiments (including live-cell imaging and vesicle tracking), samples were processed using a confocal laser scanning microscope TCS SP8-HCS (Leica, Mannheim, Germany) equipped with a Plan APO CS2 63×/1.3 NA water immersion objective. Images were acquired with a 90% open pinhole to compensate for thermal drift and active hardware autofocus. Cells were imaged in a K-Frame OKO-LABS stage-top incubator with 5% CO_2 at 37°C.

Electron microscopy

BON cells treated with scrambled shRNA or p0071 shRNA were seeded on glow discharged, carbon-coated sapphire discs (3 mm in diameter, 160 µm thick, Engineering Office M. Wohlwend GmbH, Sennwald, Switzerland) for 24 h (37°C, 5% CO_2). Cells were then high-pressure frozen using a Wohlwend HPF Compact 01 high-pressure freezer (Engineering Office M. Wohlwend GmbH) as described previously (Buser and Walther, 2008). Subsequently, samples were freeze-substituted by replacing the ice in the samples with substitution medium containing glutaraldehyde (3%), uranyl acetate (0.1%) and water (1.2%) in acetone. During freeze substitution, the temperature was slowly increased from 183 K to 273 K over a time period of 18 h. Afterwards the samples were kept at room temperature for 30 min before they were washed twice with acetone and embedded in epon (72 h, polymerization at 333 K), before sections were cut with an ultramicrotome (Leica Ultracut UCT ultramicrotome) using a diamond knife (Diatome, Biel, Switzerland). Imaging was performed with a JEOL JEM2100F.

Cell lysis, SDS-PAGE and western blotting

For western blot analysis, cells were lysed in 10 mM Tris-HCl, 5 mM EDTA, 50 mM NaCl, 50 mM NaF and 1% Triton X-100 supplemented with Complete Protease inhibitor Cocktail and PhosStop tablets (Roche, Basel, Switzerland) and, when indicated, subsequently subjected to immunoprecipitation using 2 µg of antibody and Protein-A–Sepharose (GE Healthcare, Chicago, IL). For immunoblotting, proteins were transferred to PVDF (Millipore, Billerica, MA) and nitrocellulose (GE Healthcare) membranes, respectively, after SDS-PAGE. Membranes were blocked with 5% non-fat dry milk in phosphate-buffered saline (PBS) containing 0.2% Tween 20 and incubated overnight at 4°C with specific antibodies. Antibodies used for immunoprecipitation and western blot detection include antibodies against p0071, KIF3B, PKD2, KAP3, Flag-M2, α-tubulin, acetylated tubulin, V5 epitope and β-actin. A full list of primary antibodies including dilution, catalog numbers vendors and literature references is available in Table S1. After incubation with primary antibody, membranes were extensively washed, incubated with secondary horseradish peroxidase (HRP)-conjugated antibodies (GE Healthcare) and developed using enhanced chemoluminescence substrate (Super Signal West® extended duration substrate, Thermo Scientific, Carlsbad, CA). Where indicated, western blot band intensities were quantified by using ImageJ software (Schneider et al., 2012).

Pulldown

p0071 deletion constructs [p0071-R(510-993)-pGex5.1 (armadillo repeat domain), p0071-head(1-509)-pGex5.1 (N-terminal head domain), p0071 (tail)-pGex5.1 (C-terminal tail domain)] and KAP3-pGEX-6P3 were expressed in BL21DE3 bacteria (New England Biolabs) followed by induction at A_{600}=0.6 with 1 mM isopropyl 1-thio-β-D-galactopyranoside (Thermo Scientific, Waltham, MA) for 5 h at room temperature. After lysis of bacteria, proteins were purified using glutathione–Sepharose 4B™ (GE Healthcare). For pulldown of p0071-domain-binding proteins from total cell lysate, 20 µl of beads were incubated with 1.5 mg of cell lysate from HEK293T cells transfected with overexpression constructs and empty vector, respectively. GST-loaded beads were used as negative controls. After several washing steps, beads were boiled in SDS sample buffer at 95°C and eluates subjected to SDS-PAGE and western blotting. Nitrocellulose membranes were stained for protein by incubating in Ponceau S solution (AppliChem, Darmstadt, Germany), for 5 min and destained with double-distilled H_2O. For *in vitro* binding studies of isolated proteins in a completely cell-free system, KAP3–GST was bacterially expressed in induced BL21 cells and, after bacterial lysis and purification using glutathione–Sepharose 4B™ (GE Healthcare), the purified protein was eluted from the beads using 20 mM reduced glutathione in 50 mM Tris-HCl pH 8.0. Eluates were concentrated and re-buffered to 25 mM Tris-HCl pH 8.0 using Vivaspin2 concentrators (10,000 MWCO, Satorius Stedim Biotech). The GST-tag was removed by adding 1.5 units of HRV3C protease (MoBiTec, Goettingen, Germany) per 100 µg of protein for 8 h. The protein was then incubated with glutathione beads three times for 1 hour to remove the cut tag and residual uncut GST fusion protein as well as the protease. Proper removal of the GST tag from the fusion protein was verified by SDS-PAGE and Coomassie staining using PlusOne Coomassie tablets (PhastGel Blue R-350, GE Healthcare) according to the manufacturer's instructions. p0071-head domain protein, KAP3 and GST alone were bound to glutathione–Sepharose 4B™ beads (GE Healthcare) and eluted using L-glutathione (Sigma-Aldrich). Eluates were concentrated and re-buffered to PBS using Vivaspin2 concentrators (10,000 MWCO, Satorius Stedim Biotech). Purified proteins were then mixed as indicated, incubated overnight with specific antibody against KAP3 and pulled down with protein A–Sepharose beads followed by western blot analysis.

VSV-G secretion assay

HeLa cells were stably transduced to express control shRNA and p0071 shRNA, respectively. Cells were transfected with a construct encoding a temperature-sensitive eGFP-tagged variant of VSV-Glycoprotein (Pusapati et al., 2010) and cultured at 39.5°C overnight. Cells were then incubated at 20°C for 2 h and returned to the permissive temperature (32°C) in the presence of 20 µM cycloheximide for live-cell imaging (one frame every

4 min 45 s). Fluorescence intensities over time were quantified in 10 cells per condition by measuring eGFP signals in a defined region of interest drawn around the visibly accumulated protein in the trans-Golgi area using the ImageJ software (Schneider et al., 2012).

CgA secretion assay

Stably transduced BON cells were seeded into six-well plates and starved of fetal calf serum overnight, before fresh culture medium was added to monitor secretion for 4 h. Supernatants were subjected to an ELISA using NUNC MaxiSorp™ high protein-binding capacity polystyrene 96 well ELISA plates and anti-CgA mouse monoclonal antibody (DAKO, St Clara, CA). Absorption values were determined using a microplate reader (Tecan Infinite M200 Pro, Tecan, Maennedorf, Switzerland) measuring excitation at 450 nm.

MMP9 secretion assay

Panc1 cells transduced with shRNA-expressing constructs were seeded in six-well dishes and growth medium was replaced with serum-free medium the following day. After 48 h of secretion, supernatants were collected and subjected to ELISA using a commercial kit (MMP9 Human ELISA Kit; Life Technologies, Carlsbad, CA) according to the manufacturer's instructions.

CgA time-lapse microscopy

BON cells expressing the respective shRNAs were transiently transfected with CgA–eGFP and cultivated in serum free medium at 18°C overnight to induce cargo retention at the TGN. Secretion was re-initiated by further cultivating the cells at 37°C in a live microscopy chamber. Images were acquired at time points t=0, 5, 10, 15, 20 and 25 min. Subsequently, intensities were analyzed by defining a rectangular region of interest (ROI) including the entire cell. Mean of ROI intensities were quantified with NIH ImageJ software (Schneider et al., 2012).

Vesicle tracking

To track intracellular vesicle movements, BON (or Panc1) cells expressing control shRNA or shRNA directed against p0071 and KIF3B, respectively, were transiently transfected with a construct encoding CgA–eGFP and treated with 100 nM SiR–tubulin (Spirochrome, Stein am Rhein, Germany) to stain microtubules. Cargo retention was induced at 18°C, after which cells were subjected to live imaging at 37°C (one frame every 1.29265 s) and vesicles were tracked in the cytoplasmic area between Golgi membranes and the plasma membrane by using the ImageJ manual Tracking tool (Schindelin et al., 2015). Vesicles were tracked for up to 100 frames in registered image series, dependent on the time each tracked vesicle was continuously moving within the focused layer (and thus observable). Tracking results were analyzed with help of the ibidi chemotaxis and migration tool v2.0 to calculate and visualize vesicle directional persistence.

Microtubule plus-end tracking with EB3-eGFP

End-binding-protein mEOS–EB3 was transiently expressed in HeLa cells to visualize microtubule polymerization at plus-ends. Video images were acquired at one frame per second. Fifty particles per condition were tracked by using the ImageJ manual tracking tool (Schindelin et al., 2015) over a time span of 5 s and velocities were quantified.

In vitro microtubule-binding assay

In vitro binding studies with purified microtubules were performed using the microtubule spin-down kit (#BK029, Cytoskeleton Inc., Denver, CO) according to the manufacturer's instructions. KIF3B–Flag protein for assays was affinity purified from lysate of 25 10-cm dishes of transfected HEK293 cells using FlagM2 Sepharose (Sigma-Aldrich) after previous treatment of cells with control shRNA and p0071-directed shRNA, respectively. Protein was eluted from beads by pH shift (glycine buffer pH 2.6) and concentrated as well as re-buffered in HEPES with Vivaspin2 concentrators (10,000 MWCO, Satorius Stedim Biotech). We used 2 µg of KIF3B–Flag protein per sample for microtubule-binding assays. Tubulin (100 µg) with added GTP was allowed to form polymers of ∼10 µm in length (concentration 5×10^{11} microtubules/ml) and stabilized with taxol according to the manufacturer's instructions. After incubation with KIF3B–Flag from p0071-depleted, control cells or microtubule-binding control proteins (BSA and MAP2, respectively), samples were loaded onto cushion buffer (80 mM PIPES, 1 mM $MgCl_2$, 1 mM EGTA, 60% glycerol) and subjected to a 100,000 ***g*** ultracentrifugation. Fractions were then analyzed by western blotting and quantified as stated in the respective figure legend.

Statistical analysis

Statistical analysis was performed using Prism software, version 6.00, for Windows (GraphPad, San Diego, CA). Graphs depict mean±s.e.m. for all conditions. Statistical significance: ns, not significant, *P=0.05–0.01, **P=0.01–0.001, ***P<0.001, ****P<0.0001.

Acknowledgements

The authors want to acknowledge use of the Imaging Core Facility for 'Multiphoton and Confocal Microscopy' at Ulm University. We thank Franz Oswald (Ulm University) for providing valuable research materials and Ninel Azoitei for critically reading the manuscript.

Competing interests

The authors declare no competing or financial interests.

Author contributions

Conceptualization: T.E., T.S.; Methodology: A.B., T.E., M.P., P.W., R.K., S.B.; Formal analysis: A.B., T.E., M.P., P.W., T.S.; Investigation: A.B., T.E., M.P., S.B.; Resources: R.K., M.H., T.S.; Writing - original draft: A.B., T.E., P.W., M.H., T.S.; Visualization: A.B., T.E.; Supervision: T.E., T.S.; Project administration: T.S.; Funding acquisition: A.B., T.E., T.S.

Funding

This work was funded by the Deutsche Forschungsgemeinschaft [EI792/3-1 to T.E., SE 676/10-1 to T.S.] and the the International Graduate School in Molecular Medicine at Ulm University to A.B.

Supplementary information

Supplementary information available online at
http://jcs.biologists.org/lookup/doi/10.1242/jcs.200170.supplemental

References

Akhmanova, A. and Steinmetz, M. O. (2008). Tracking the ends: a dynamic protein network controls the fate of microtubule tips. *Nat. Rev. Mol. Cell Biol.* **9**, 309-322.

Albracht, C. D., Guzik-Lendrum, S., Rayment, I. and Gilbert, S. P. (2016). Heterodimerization of kinesin-2 KIF3AB modulates entry into the processive run. *J. Biol. Chem.* **291**, 23248-23256.

Alema, S. and Salvatore, A. M. (2007). p120 catenin and phosphorylation: Mechanisms and traits of an unresolved issue. *Biochim. Biophys. Acta* **1773**, 47-58.

Asthana, J., Kapoor, S., Mohan, R. and Panda, D. (2013). Inhibition of HDAC6 deacetylase activity increases its binding with microtubules and suppresses microtubule dynamic instability in MCF-7 cells. *J. Biol. Chem.* **288**, 22516-22526.

Blehm, B. H. and Selvin, P. R. (2014). Single-molecule fluorescence and in vivo optical traps: how multiple dyneins and kinesins interact. *Chem. Rev.* **114**, 3335-3352.

Buser, C. and Walther, P. (2008). Freeze-substitution: the addition of water to polar solvents enhances the retention of structure and acts at temperatures around −60°C. *J. Microsc.* **230**, 268-277.

Cai, D., McEwen, D. P., Martens, J. R., Meyhofer, E. and Verhey, K. J. (2009). Single molecule imaging reveals differences in microtubule track selection between Kinesin motors. *PLoS Biol.* **7**, e1000216.

Chabin-Brion, K., Marceiller, J., Perez, F., Settegrana, C., Drechou, A., Durand, G. and Pous, C. (2001). The Golgi complex is a microtubule-organizing organelle. *Mol. Biol. Cell* **12**, 2047-2060.

De Rossi, M. C., De Rossi, M. E., Sued, M., Rodríguez, D., Bruno, L. and Levi, V. (2015). Asymmetries in kinesin-2 and cytoplasmic dynein contributions to melanosome transport. *FEBS Lett.* **589**, 2763-2768.

Deacon, S. W., Serpinskaya, A. S., Vaughan, P. S., Lopez Fanarraga, M., Vernos, I., Vaughan, K. T. and Gelfand, V. I. (2003). Dynactin is required for bidirectional organelle transport. *J. Cell Biol.* **160**, 297-301.

Doodhi, H., Ghosal, D., Krishnamurthy, M., Jana, S. C., Shamala, D., Bhaduri, A., Sowdhamini, R. and Ray, K. (2009). KAP, the accessory subunit of kinesin-2, binds the predicted coiled-coil stalk of the motor subunits. *Biochemistry* **48**, 2248-2260.

Egeblad, M. and Werb, Z. (2002). New functions for the matrix metalloproteinases in cancer progression. *Nat. Rev. Cancer* **2**, 161-174.

Journal of Cell Science

Eiseler, T., Wille, C., Koehler, C., Illing, A. and Seufferlein, T. (2016). Protein kinase D2 assembles a multiprotein complex at the trans-golgi network to regulate matrix metalloproteinase secretion. *J. Biol. Chem.* **291**, 462-477.

Elias, S., Delestre, C., Ory, S., Marais, S., Courel, M., Vazquez-Martinez, R., Bernard, S., Coquet, L., Malagon, M. M., Driouich, A. et al. (2012). Chromogranin A induces the biogenesis of granules with calcium- and actin-dependent dynamics and exocytosis in constitutively secreting cells. *Endocrinology* **153**, 4444-4456.

Erickson, L. E. (1980). Inhibition of intracellular protein transport in the mouse exocrine pancreas induced by vinblastine. *Cell Tissue Res.* **206**, 73-81.

Evers, B. M., Ishizuka, J., Townsend, C. M., Jr and Thompson, J. C. (1994). The human carcinoid cell line, BON. A model system for the study of carcinoid tumors. *Ann. N. Y. Acad. Sci.* **733**, 393-406.

Fu, M.-M. and Holzbaur, E. L. F. (2013). JIP1 regulates the directionality of APP axonal transport by coordinating kinesin and dynein motors. *J. Cell Biol.* **202**, 495-508.

Gross, S. P., Welte, M. A., Block, S. M. and Wieschaus, E. F. (2002). Coordination of opposite-polarity microtubule motors. *J. Cell Biol.* **156**, 715-724.

Hanania, R., Sun, H. S., Xu, K., Pustylnik, S., Jeganathan, S. and Harrison, R. E. (2012). Classically activated macrophages use stable microtubules for matrix metalloproteinase-9 (MMP-9) secretion. *J. Biol. Chem.* **287**, 8468-8483.

Hatzfeld, M. (2005). The p120 family of cell adhesion molecules. *Eur. J. Cell Biol.* **84**, 205-214.

Hatzfeld, M. and Nachtsheim, C. (1996). Cloning and characterization of a new armadillo family member, p0071, associated with the junctional plaque: evidence for a subfamily of closely related proteins. *J. Cell Sci.* **109**, 2767-2778.

Hendricks, A. G., Perlson, E., Ross, J. L., Schroeder, H. W., III, Tokito, M. and Holzbaur, E. L. F. (2010). Motor coordination via a tug-of-war mechanism drives bidirectional vesicle transport. *Curr. Biol.* **20**, 697-702.

Hill, D. B., Plaza, M. J., Bonin, K. and Holzwarth, G. (2004). Fast vesicle transport in PC12 neurites: velocities and forces. *Eur. Biophys. J.* **33**, 623-632.

Hirokawa, N., Noda, Y., Tanaka, Y. and Niwa, S. (2009). Kinesin superfamily motor proteins and intracellular transport. *Nat. Rev. Mol. Cell Biol.* **10**, 682-696.

Jakobsen, K. R., Sørensen, E., Brøndum, K. K., Daugaard, T. F., Thomsen, R. and Nielsen, A. L. (2013). Direct RNA sequencing mediated identification of mRNA localized in protrusions of human MDA-MB-231 metastatic breast cancer cells. *J. Mol. Signal.* **8**, 9.

Jimbo, T., Kawasaki, Y., Koyama, R., Sato, R., Takada, S., Haraguchi, K. and Akiyama, T. (2002). Identification of a link between the tumour suppressor APC and the kinesin superfamily. *Nat. Cell Biol.* **4**, 323-327.

Joseph, R. A., Shepard, B. D., Kannarkat, G. T., Rutledge, T. M., Tuma, D. J. and Tuma, P. L. (2008). Microtubule acetylation and stability may explain alcohol-induced alterations in hepatic protein trafficking. *Hepatology* **47**, 1745-1753.

Keil, R. and Hatzfeld, M. (2014). The armadillo protein p0071 is involved in Rab11-dependent recycling. *J. Cell Sci.* **127**, 60-71.

Keil, R., Wolf, A., Huettelmaier, S. and Hatzfeld, M. (2007). Beyond regulation of cell adhesion: local control of RhoA at the cleavage furrow by the p0071 catenin. *Cell Cycle* **6**, 122-127.

Keil, R., Kiessling, C. and Hatzfeld, M. (2009). Targeting of p0071 to the midbody depends on KIF3. *J. Cell Sci.* **122**, 1174-1183.

Keil, R., Schulz, J. and Hatzfeld, M. (2013). p0071/PKP4, a multifunctional protein coordinating cell adhesion with cytoskeletal organization. *Biol. Chem.* **394**, 1005-1017.

Kondo, S., Sato-Yoshitake, R., Noda, Y., Aizawa, H., Nakata, T., Matsuura, Y. and Hirokawa, N. (1994). KIF3A is a new microtubule-based anterograde motor in the nerve axon. *J. Cell Biol.* **125**, 1095-1107.

Kreitzer, G., Marmorstein, A., Okamoto, P., Vallee, R. and Rodriguez-Boulan, E. (2000). Kinesin and dynamin are required for post-Golgi transport of a plasma-membrane protein. *Nat. Cell Biol.* **2**, 125-127.

Luby-Phelps, K., Castle, P. E., Taylor, D. L. and Lanni, F. (1987). Hindered diffusion of inert tracer particles in the cytoplasm of mouse 3T3 cells. *Proc. Natl. Acad. Sci. USA* **84**, 4910-4913.

McCrea, P. D. and Gu, D. (2010). The catenin family at a glance. *J. Cell Sci.* **123**, 637-642.

Münzberg, C., Höhn, K., Krndija, D., Maass, U., Bartsch, D. K., Slater, E. P., Oswald, F., Walther, P., Seufferlein, T. and von Wichert, G. (2015). IGF-1 drives chromogranin A secretion via activation of Arf1 in human neuroendocrine tumour cells. *J. Cell. Mol. Med.* **19**, 948-959.

Nolze, A., Schneider, J., Keil, R., Lederer, M., Huttelmaier, S., Kessels, M. M., Qualmann, B. and Hatzfeld, M. (2013). FMRP regulates actin filament organization via the armadillo protein p0071. *RNA* **19**, 1483-1496.

Patel, S., Wetie, A. G. N., Darie, C. C. and Clarkson, B. D. (2014). Cancer secretomes and their place in supplementing other hallmarks of cancer. *Adv. Exp. Med. Biol.* **806**, 409-442.

Pusapati, G. V., Krndija, D., Armacki, M., von Wichert, G., von Blume, J., Malhotra, V., Adler, G. and Seufferlein, T. (2010). Role of the second cysteine-rich domain and Pro275 in protein kinase D2 interaction with ADP-ribosylation factor 1, trans-Golgi network recruitment, and protein transport. *Mol. Biol. Cell* **21**, 1011-1022.

Schackmann, R. C. J., Tenhagen, M., van de Ven, R. A. H. and Derksen, P. W. B. (2013). p120-catenin in cancer - mechanisms, models and opportunities for intervention. *J. Cell Sci.* **126**, 3515-3525.

Schindelin, J., Rueden, C. T., Hiner, M. C. and Eliceiri, K. W. (2015). The ImageJ ecosystem: An open platform for biomedical image analysis. *Mol. Reprod. Dev.* **82**, 518-529.

Schneider, C. A., Rasband, W. S. and Eliceiri, K. W. (2012). NIH Image to ImageJ: 25 years of image analysis. *Nat. Methods* **9**, 671-675.

Scholey, J. M. (2013). Kinesin-2: a family of heterotrimeric and homodimeric motors with diverse intracellular transport functions. *Annu. Rev. Cell Dev. Biol.* **29**, 443-469.

Soppina, V., Rai, A. K., Ramaiya, A. J., Barak, P. and Mallik, R. (2009). Tug-of-war between dissimilar teams of microtubule motors regulates transport and fission of endosomes. *Proc. Natl. Acad. Sci. USA* **106**, 19381-19386.

Sroka, R., Van Lint, J., Katz, S.-F., Schneider, M. R., Kleger, A., Paschke, S., Seufferlein, T. and Eiseler, T. (2016). Cortactin is a scaffolding platform for the E-cadherin adhesion complex and is regulated by protein kinase D1 phosphorylation. *J. Cell Sci.* **129**, 2416-2429.

Stauber, T., Simpson, J. C., Pepperkok, R. and Vernos, I. (2006). A role for kinesin-2 in COPI-dependent recycling between the ER and the Golgi complex. *Curr. Biol.* **16**, 2245-2251.

Takeda, S., Yamazaki, H., Seog, D.-H., Kanai, Y., Terada, S. and Hirokawa, N. (2000). Kinesin superfamily protein 3 (KIF3) motor transports fodrin-associating vesicles important for neurite building. *J. Cell Biol.* **148**, 1255-1265.

Thuret-Carnahan, J., Bossu, J. L., Feltz, A., Langley, K. and Aunis, D. (1985). Effect of taxol on secretory cells: functional, morphological, and electrophysiological correlates. *J. Cell Biol.* **100**, 1863-1874.

Verhey, K. J. and Hammond, J. W. (2009). Traffic control: regulation of kinesin motors. *Nat. Rev. Mol. Cell Biol.* **10**, 765-777.

von Wichert, G., Jehle, P. M., Hoeflich, A., Koschnick, S., Dralle, H., Wolf, E., Wiedenmann, B., Boehm, B. O., Adler, G. and Seufferlein, T. (2000). Insulin-like growth factor-I is an autocrine regulator of chromogranin A secretion and growth in human neuroendocrine tumor cells. *Cancer Res.* **60**, 4573-4581.

von Wichert, G., Haeussler, U., Greten, F. R., Kliche, S., Dralle, H., Böhm, B. O., Adler, G. and Seufferlein, T. (2005). Regulation of cyclin D1 expression by autocrine IGF-I in human BON neuroendocrine tumour cells. *Oncogene* **24**, 1284-1289.

von Wichert, G., Edenfeld, T., von Blume, J., Krisp, H., Krndija, D., Schmid, H., Oswald, F., Lother, U., Walther, P., Adler, G. et al. (2008). Protein kinase D2 regulates chromogranin A secretion in human BON neuroendocrine tumour cells. *Cell. Signal.* **20**, 925-934.

Webster, D. R. and Borisy, G. G. (1989). Microtubules are acetylated in domains that turn over slowly. *J. Cell Sci.* **92**, 57-65.

Wille, C., Kohler, C., Armacki, M., Jamali, A., Gossele, U., Pfizenmaier, K., Seufferlein, T. and Eiseler, T. (2014). Protein kinase D2 induces invasion of pancreatic cancer cells by regulating matrix metalloproteinases. *Mol. Biol. Cell* **25**, 324-336.

Wolf, A., Keil, R., Götzl, O., Mun, A., Schwarze, K., Lederer, M., Hüttelmaier, S. and Hatzfeld, M. (2006). The armadillo protein p0071 regulates Rho signalling during cytokinesis. *Nat. Cell Biol.* **8**, 1432-1440.

Xie, R., Nguyen, S., McKeehan, W. L. and Liu, L. (2010). Acetylated microtubules are required for fusion of autophagosomes with lysosomes. *BMC Cell Biol.* **11**, 89.

Yamazaki, H., Nakata, T., Okada, Y. and Hirokawa, N. (1995). KIF3A/B: a heterodimeric kinesin superfamily protein that works as a microtubule plus end-directed motor for membrane organelle transport. *J. Cell Biol.* **130**, 1387-1399.

Yamazaki, H., Nakata, T., Okada, Y. and Hirokawa, N. (1996). Cloning and characterization of KAP3: a novel kinesin superfamily-associated protein of KIF3A/3B. *Proc. Natl. Acad. Sci. USA* **93**, 8443-8448.

Supplementary Information

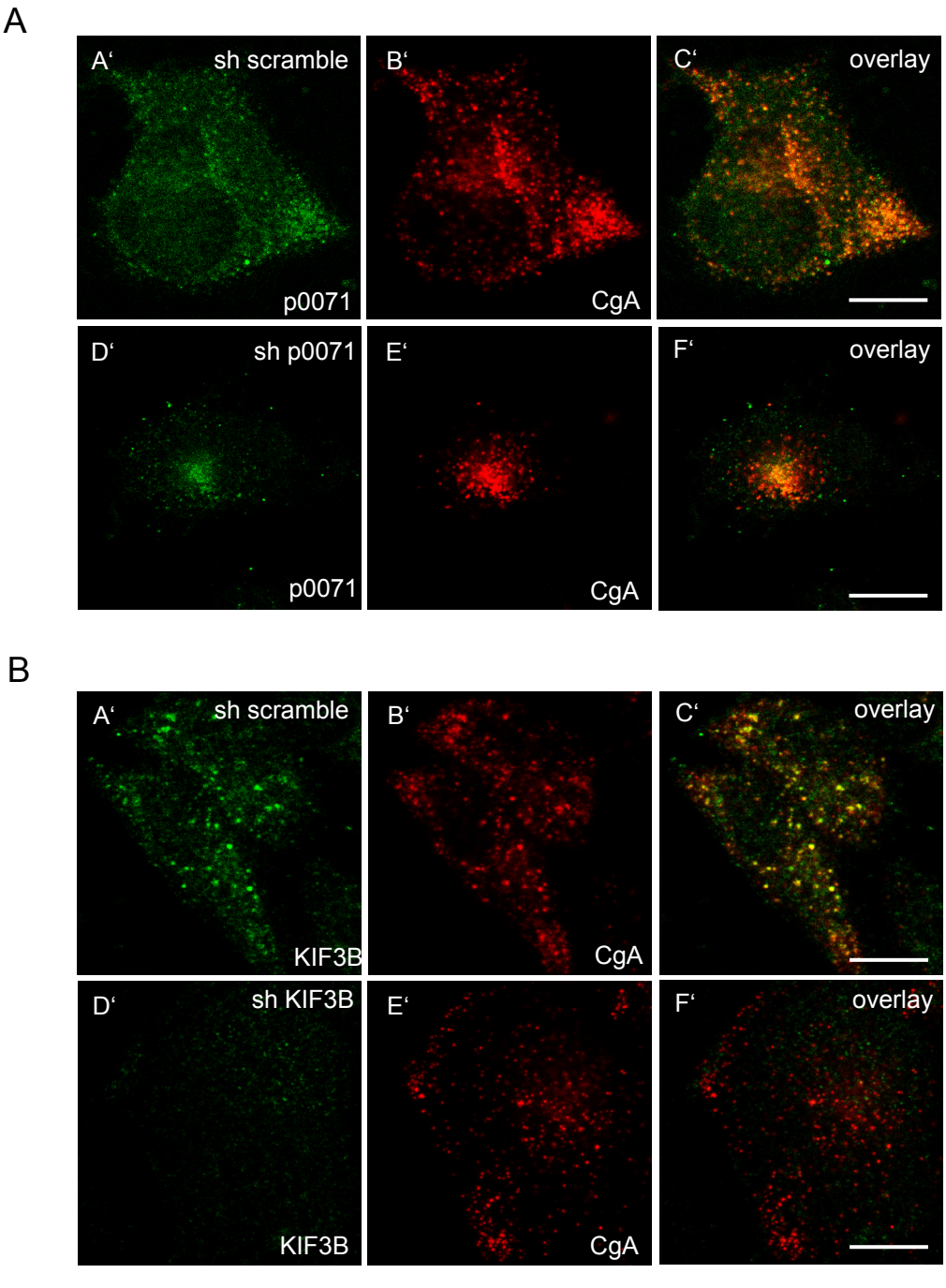

Fig. S1. Specificity of antibodies used in immunofluorescence staining. (A) Confocal image sections of BON cells treated with control or p0071- targeted shRNA, fixed and stained with antibodies against p0071 and chromogranin A. The specific localization of p0071 as described in Fig. 1B is lost upon p0071 depletion despite a weak residual staining in the perinuclear area. Scale bar: 10μm (B) Confocal image sections of BON cells stained for KIF3B and CgA. Signal intensity and specific co-localization of KIF3B with CgA-positive vesicles is lost upon knockdown of KIF3B. Scale bar: 10μm.

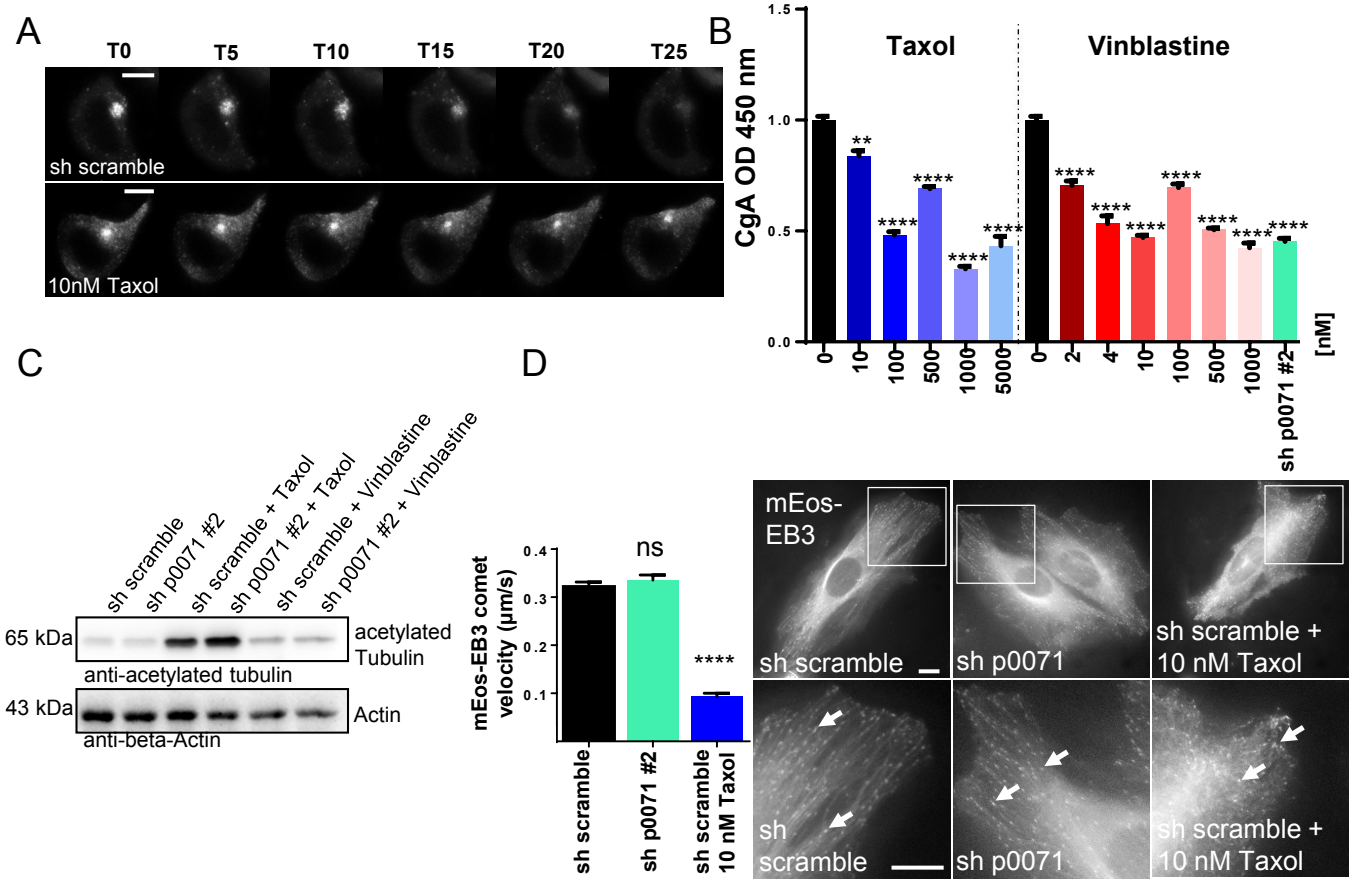

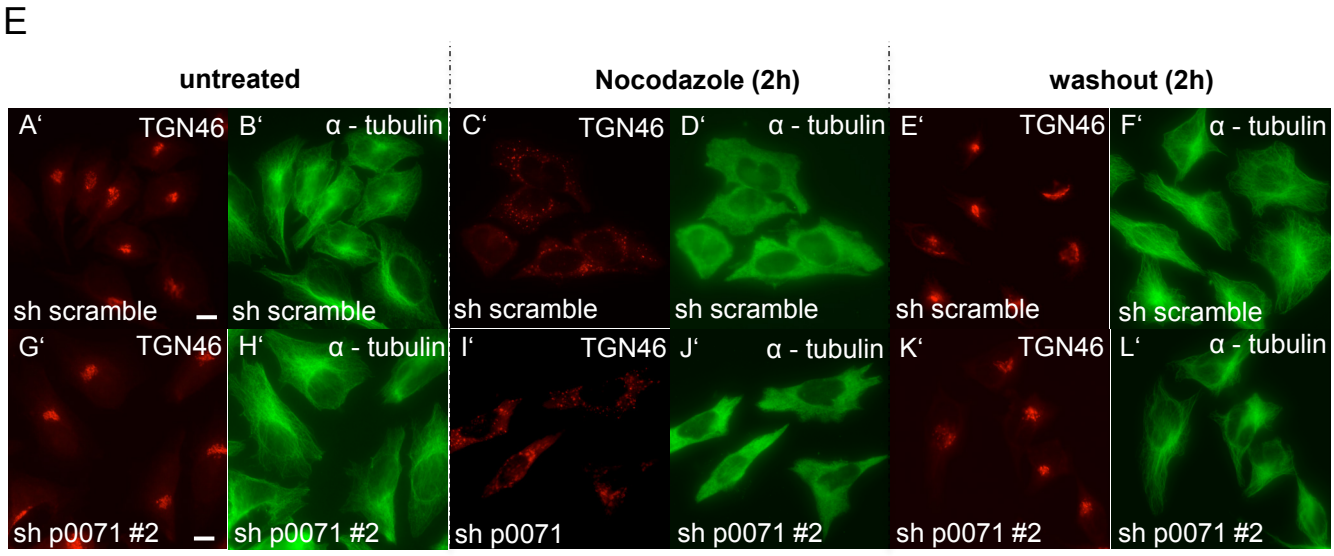

Fig. S2. P0071 depletion does not affect microtubule network and Golgi organization. (A) CgA-GFP time-lapse microscopy in BON cells. Images have been extracted from a live cell video series showing intracellular fluorescence intensity of CgA-GFP after temperature-mediated block at the TGN and subsequent re-initiation of secretion over a time period of 25 minutes. Incubation of BON cells with 10nM taxol impaired CgA release indicated by enhanced intracellular CgA-GFP fluorescence after 25 minutes. The control cell with scrambled shRNA (upper panel) is also depicted in Fig. 2A as part of an experiment performed together with the taxol treatment. Scale bars: 7.5µm. (B) Treatment of BON cells with microtubule targeting agents taxol and vinblastine impairs CgA secretion. BON cells were incubated over night with the indicated doses of drugs, and effects were compared to p0071 knockdown. Mean and SEM from n=6 experiments. $^{**}P<0.01$, $^{****}P<0.0001$ (two-tailed unpaired Student's *t*-test). (C) Knockdown of p0071 in HeLa cells does not change alpha-tubulin acetylation, in contrast to taxol (10nM) or vinblastine (5nM), as shown by western blot and an acetylation specific antibody. (D) End-binding protein mEOS-EB3 tracking microcopy. mEOS-EB3 was transiently expressed in HeLa cells to monitor microtubule plus-end polymerization. Cells treated with p0071 shRNA were compared to control cells and cells incubated with taxol (10nM) over night (see images in right panel). Fifty particles per condition were tracked over 5 seconds and velocities were quantified (left panel). The graph represents mean and SEM, $^{****}P<0.0001$ (two-tailed unpaired Student's *t*-test). (E) Nocodazole washout experiments in HeLa cells. HeLa cells (treated with control shRNA and shp0071, respectively) were exposed to nocodazole for 2 hours before intensive washout. Cells were fixed and stained for alpha-tubulin (green) and the TGN marker TGN46 (red) before treatment, after incubation with nocodazole and at 2 hours following washout. Golgi disruption and microtubule organization after nocodazole treatment and after re-organization following washout is shown for all samples.

Figure S3

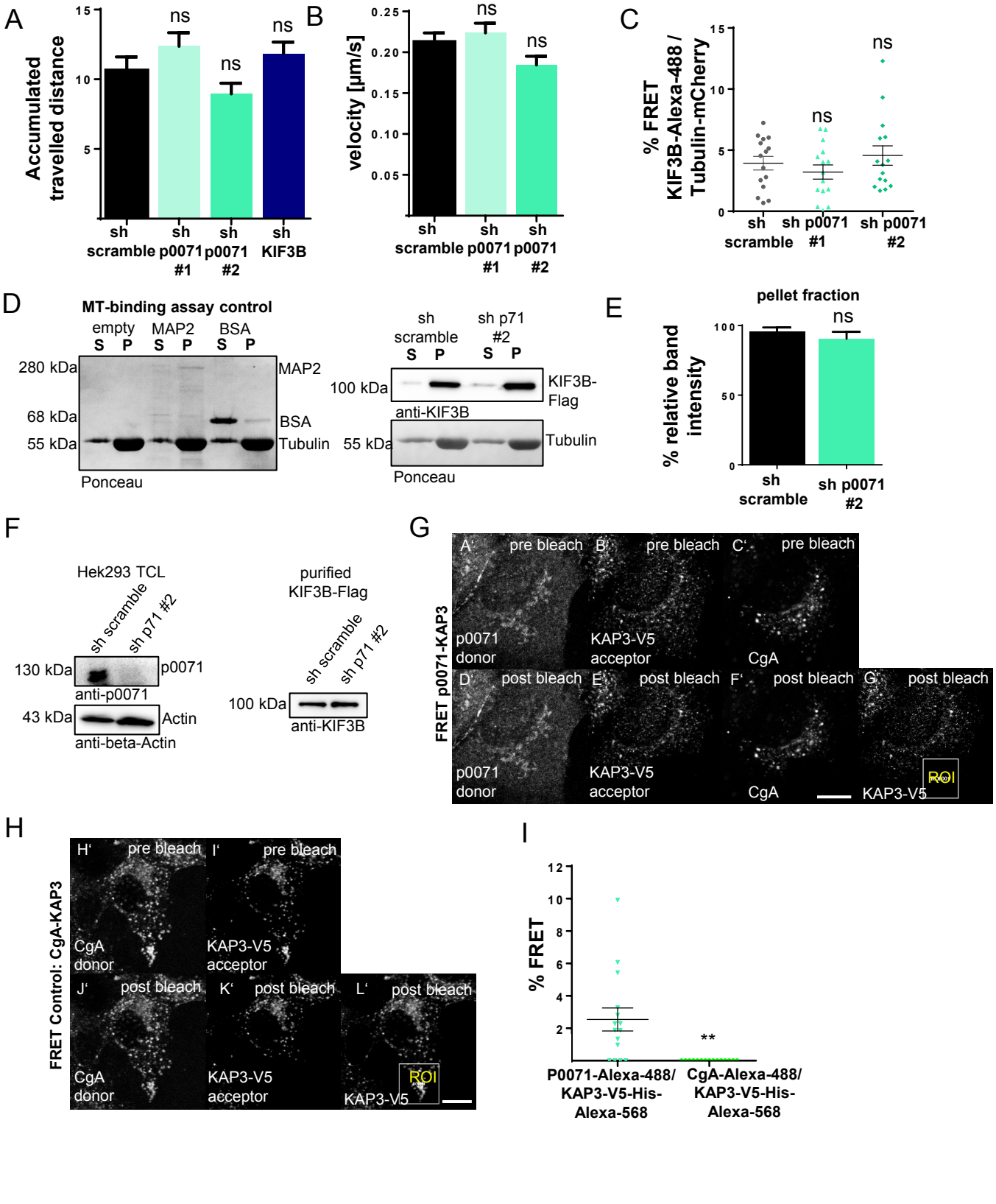

Fig. S3. Molecular interactions of KIF3 complex proteins. (A) Accumulated distance (accounting for movement in both directions from the tracking starting point) of CgA-GFP vesicles in BON cells traced in live cell imaging videos quantified in Fig. 5 A-C. Forty tracks per condition (control shRNA; shp0071 # 1&2; shKif3B) were observed and quantified for as long as they were present in the focus layer. (B) Velocities of vesicles in BON cells treated with control shRNA and shp0071, respectively, were quantified as described in A). Velocities are shown in µm per second. (C) Binding of the KIF3B motor proteins to microtubules. Quantitative AB-FRET analysis of KIF3B labeled by Alexa-488 dye and transiently expressed alpha-tubulin-mCherry in BON cells treated with scrambled shRNA or two different shRNAs directed against p0071, respectively. The graph shows the mean and SEM %FRET (*n*=15 cells and three independent experiments). ns, not significant (two-tailed unpaired Student's *t*-test). (D) Left-hand side: Microtubule binding spin-down assay control experiment showing specific interaction of the microtubule associated protein MAP2A and BSA as negative control. Right-hand side: Microtubule binding assay performed with KIF3B-Flag protein purified from control cells and cells depleted of p0071, respectively. (E) Statistical analysis of KIF3B-Flag amount detected in pellet fractions relative to total amount of KIF3B-Flag used in assays (pellet + sup). Integrated band intensities from n=3 experiments; ns, no significant differences in KIF3 complex binding to microtubules. (F) Left-hand side: Verification of p0071 knockdown in Hek293 cells used for KIF3B-Flag expression and purification. Right-hand side: Western blot of KIF3B-Flag protein used for microtubule binding studies shown in D) and E). (G) Interaction of endogenous p0071 labeled by anti-p0071 and Alexa-488 antibodies (donor; A'; D') with KAP3-V5-His probed by anti-V5 and Alexa-568 secondary antibodies (acceptor; B'; E'). Interaction was quantified by AB-FRET in the cytosolic region of BON cells containing CgA granula stained by anti-CgA and Alexa-647 antibodies (C'; F'). The bleach-region (ROI) is shown in (G'). Scale bar: 10 µm (H) The cargo CgA contained in vesicles labeled by anti-CgA and Alexa-488 antibodies was used a non-interacting negative control for FRET experiments together with KAP3-V5-His stained by anti-V5 and Alexa-568 antibodies (H' to K', the bleach- ROI is shown in (L'). Scale bar: 10 µm. (I) Statistical analysis of 15 cells from G and H. Mean and SEM %FRET; ns, non significant (two-tailed unpaired Student's *t*-test).

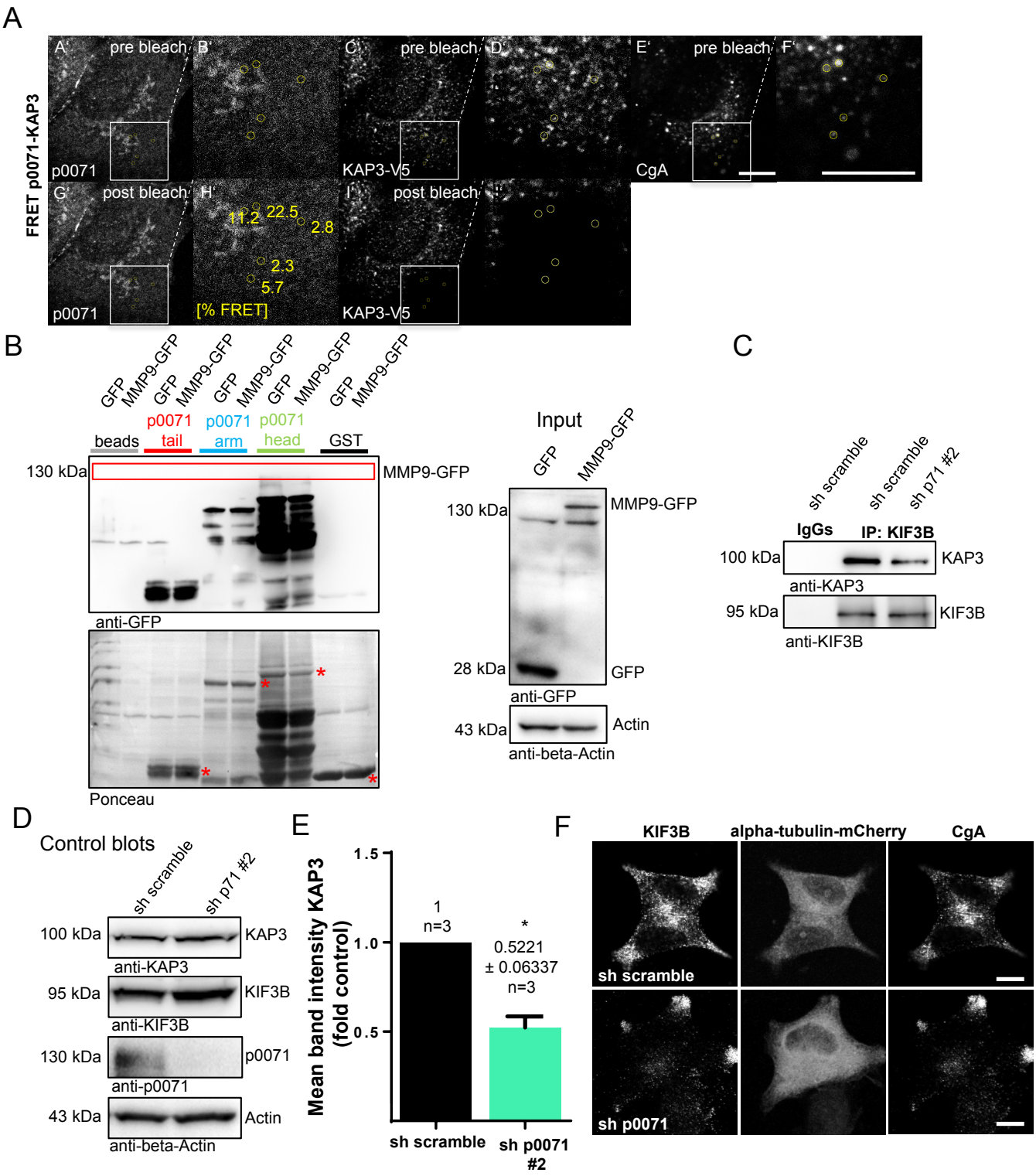

Fig. S4. KAP3 and p0071 binding studies. (A) Representative Sub-ROI analysis for the interaction of p0071 (A'; G'; magnifications B' and H', respectively) and KAP3-V5-His (C'; I'; magnifications D' and J', respectively) at vesicular structures marked by CgA staining (E'; F') in BON cells. Sub-ROIs are highlighted by yellow circles around CgA-positive structures (E'; F'). %FRET of individual Sub-ROIs is shown as yellow numbers in H'. Scale bar: 10 µm. (B) Left-hand panel: Control pulldown experiments to demonstrate lack of binding of MMP-9 to individual domains of p0071. MMP-9-GFP was expressed in HEK293T cells and cell lysates were incubated with purified GST-p0071-head, GST-p0071-armadillo repeat and GST-p0071 tail domains immobilized on GST-sepharose beads, respectively. Empty beads and GST-loaded beads as well as HEK293T lysates transfected with empty vector were used as negative controls. Ponceau staining of the respective membrane shows the presence of GST proteins. Asterisks mark the full-length GST proteins. Right-hand panel: Expression of KAP3-V5-His in HEK293T cells. (C) Co-immunoprecipitation experiments were performed as described in Fig. 7A using a second p0071-directed shRNA (shp0071 #2). KAP3 signals were normalized to the intensities of KIF3B IP bands. (D) Control blots showing protein expression in total cell lysates from cells used in C). (E) Statistical analysis of co-precipitated KAP3 in KIF3B IPs. N=3 experiments, mean and SEM, **P*<0.05 (two-tailed paired Student's *t*-test). (F) Representative images of BON cells used for KIF3B signal intensity analysis as shown in Fig. 7E, F. Cells were treated with scrambled shRNA and p0071-directed shRNA (shp0071 #1), respectively and transfected to express alpha-tubulin-mCherry . KIF3B and CgA were stained with specific primary and secondary antibodies.

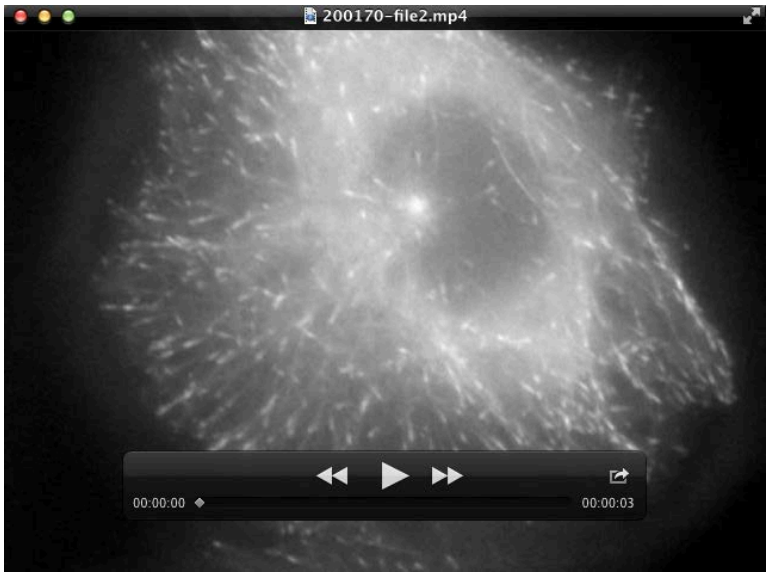

Movie S1. mEos-EB3 comet tracking in a HeLa cell. HeLa cells treated with scrambled shRNA were transfected to express mEos-EB3. End-point tracking was performed at 37°C using an inverted Olympus IX71 microscope (Olympus, Hamburg, Germany) and quantified with the ImageJ manual tracking tool (Schindelin et al., 2015).

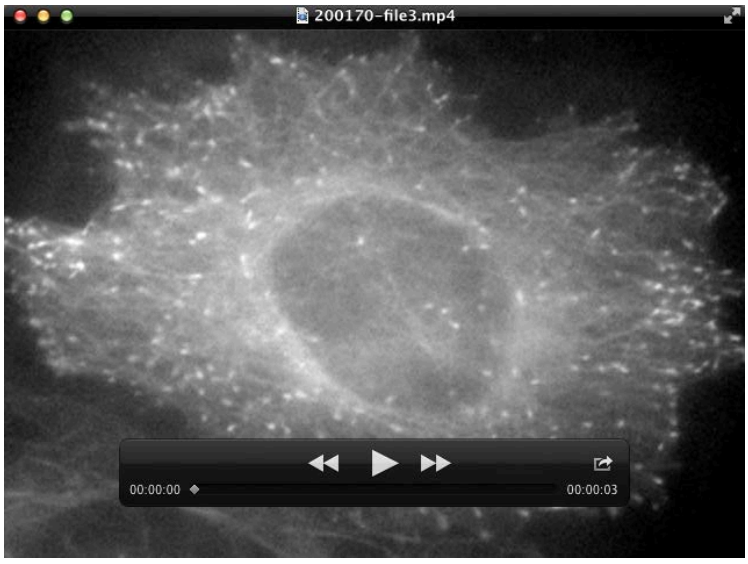

Movie S2. mEos-EB3 comet tracking in a p0071-knockdown HeLa cell. P0071 was knocked down in HeLa cells using a specific shRNA and cells were transfected to express mEos-EB3. End-point tracking was performed at 37°C using an inverted Olympus IX71 microscope (Olympus, Hamburg, Germany) and quantified with the ImageJ manual tracking tool (Schindelin et al., 2015).

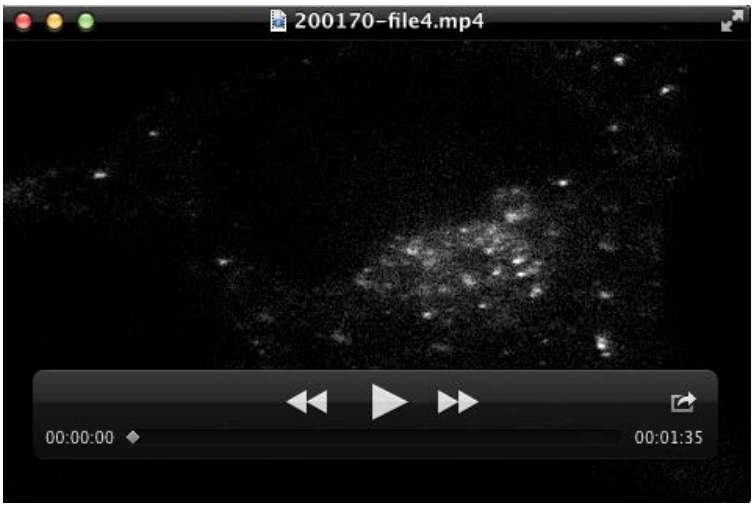

Movie S3. Movement of CgA vesicles in a BON cell. Cells were treated with scrambled shRNA and transfected to transiently express CgA-GFP. Cargo retention was induced at 18°C and re-release initiated at permissive temperature. Live imaging was carried out at 37°C using a confocal laser-scanning microscope and vesicles (seen as bright rounded structures) were tracked in several cells within the cytoplasmic area using the ImageJ manual Tracking tool (Schindelin et al., 2015).

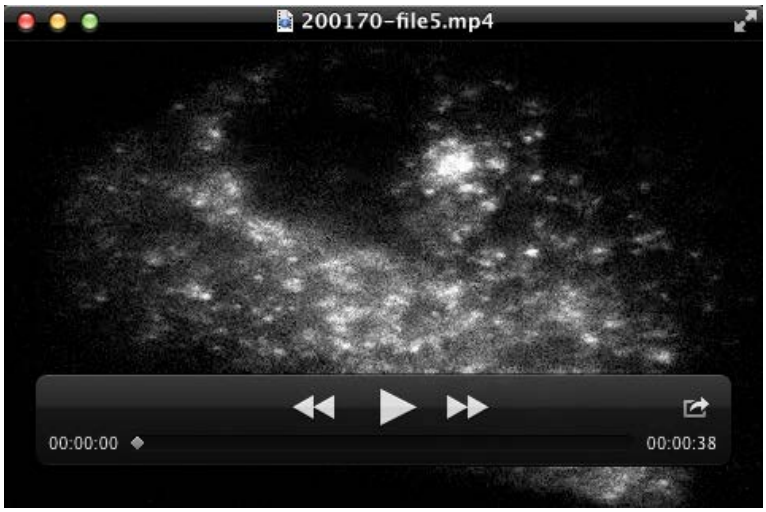

Movie S4. Erratical movement of CgA vesicles in a p0071 depleted BON cell. Cells were treated with p0071-directed shRNA and transfected to transiently express CgA-GFP. Cargo retention was induced at 18°C and re-release initiated at permissive temperature. Live imaging was carried out at 37°C using a confocal laser-scanning microscope and intracellularly accumulated CgA vesicles were tracked in several cells within the cytoplasmic area using the ImageJ manual Tracking tool (Schindelin et al., 2015).

Table S1: List of primary and secondary antibodies with ordering number, company name, dilution and references of usage. WB: Western blot, IF: Immunofluorescence, IP: Immunoprecipitation.

Name	ordering number	company	Dilution	References
p0071	GP71	Progen, Heidelberg, Germany	IF: 1:50 IP: 2µg	(Hofmann et al., 2008; Hofmann et al., 2009; Medvetz et al., 2012)
KIF3B	sc-50456	St Cruz, Santa Cruz, CA, USA	IF: 1:100 WB: 1:1000 IP: 2µg	(Aguado-Fraile et al., 2012; Keil et al., 2009)
KAP3	sc-55598	St Cruz, Santa Cruz, CA, USA	IF: 1:100 WB: 1:1000	(Landers et al., 2009; Traynor et al., 2010)
alpha-tubulin	T5168	Sigma Aldrich, St Louis, MO, USA	IF: 1:200 WB: 1:1000	(Lefave et al., 2011; Whelan et al., 2010)
TGN46	NBP1-49643	Novus Biologicals, Littleton, CO, USA	IF: 1:500	(Eiseler et al., 2016; Wille et al., 2014)
chromogranin A	M086929-2	DAKO, St Clara, CA, USA	IF: 1:100	(Aguilera et al., 2015; Gradiz et al., 2016; Scharfmann et al., 2014)
beta-actin	#A2228	Sigma Aldrich, St Louis, MO, USA	WB: 1:2000	(Darr et al., 2014; Wohlfert et al., 2006; Zhao et al., 2011)
Flag-M2	#F1804	Sigma Aldrich, St Louis, MO, USA	WB: 1:2000 IP: 2µg	(Han et al., 2010; He et al., 2010; Kinsey et al., 2009; Rudinskiy et al., 2009)
p0071	651166	Progen, Heidelberg, Germany	WB: 1:100	(Hofmann et al., 2008; Hofmann et al., 2009)
PKD2	A300-073A	Bethyl, Montgomery, TX, USA	WB: 1:1000	(Azoitei et al., 2011; Irie et al., 2012; Zheng et al., 2011)
acetylated tubulin	ab125356	Abcam, Cambridge, UK	WB: 1:1000	(Mori et al., 2015; Smirnova et al., 2016; Xiaojun et al., 2016)
V5 epitope	ab3792	Millipore, Billerica, MA, USA	WB: 1:2000	(Cui et al., 2015; Jablonski et al., 2015; Minoura et al., 2016)
Anti-guinea pig FITC	F-7762	Sigma Aldrich, St Louis, MO, USA	IF: 1:400	(Geffrotin et al., 2000; Kasimiotis et al., 2000; Makarenko et al., 2002)
Alexa-Fluor 568/647 goat-anti-rabbit	# A11036 # A21244	Thermo Scientific, Carlsbad, CA, USA	IF: 1:400	(Eiseler et al., 2010; Eiseler et al., 2012; Eiseler et al., 2015; Wille et al., 2014)
Alexa-Fluor 488/568 goat-anti-mouse	#A11029 #A11031	Thermo Scientific, Carlsbad, CA, USA	IF: 1:400	(Eiseler et al., 2010; Eiseler et al., 2012; Eiseler et al., 2015; Wille et al., 2014)
Alexa-Fluor 488 goat-anti-guinea pig	#A11073	Thermo Scientific, Carlsbad, CA, USA	IF: 1:400	(Baer et al., 2012; Checchi et al., 2014; Housley et al., 2013)

References

Aguado-Fraile, E., Ramos, E., Saenz-Morales, D., Conde, E., Blanco-Sanchez, I., Stamatakis, K., del Peso, L., Cuppen, E., Brune, B. and Bermejo, M. L. (2012). miR-127 protects proximal tubule cells against ischemia/reperfusion: identification of kinesin family member 3B as miR-127 target. *PLoS One* **7**, e44305.

Aguilera, O., Gonzalez-Sancho, J. M., Zazo, S., Rincon, R., Fernandez, A. F., Tapia, O., Canals, F., Morte, B., Calvanese, V., Orgaz, J. L. et al. (2015). Nuclear DICKKOPF-1 as a biomarker of chemoresistance and poor clinical outcome in colorectal cancer. *Oncotarget* **6**, 5903-17.

Azoitei, N., Kleger, A., Schoo, N., Thal, D. R., Brunner, C., Pusapati, G. V., Filatova, A., Genze, F., Moller, P., Acker, T. et al. (2011). Protein kinase D2 is a novel regulator of glioblastoma growth and tumor formation. *Neuro Oncol* **13**, 710-24.

Baer, M. M., Palm, W., Eaton, S., Leptin, M. and Affolter, M. (2012). Microsomal triacylglycerol transfer protein (MTP) is required to expand tracheal lumen in Drosophila in a cell-autonomous manner. *J Cell Sci* **125**, 6038-48.

Checchi, P. M., Lawrence, K. S., Van, M. V., Larson, B. J. and Engebrecht, J. (2014). Pseudosynapsis and decreased stringency of meiotic repair pathway choice on the hemizygous sex chromosome of Caenorhabditis elegans males. *Genetics* **197**, 543-60.

Cui, J., Xiao, J., Tagliabracci, V. S., Wen, J., Rahdar, M. and Dixon, J. E. (2015). A secretory kinase complex regulates extracellular protein phosphorylation. *Elife* **4**, e06120.

Darr, J., Klochendler, A., Isaac, S. and Eden, A. (2014). Loss of IGFBP7 expression and persistent AKT activation contribute to SMARCB1/Snf5-mediated tumorigenesis. *Oncogene* **33**, 3024-32.

Eiseler, T., Hausser, A., De Kimpe, L., Van Lint, J. and Pfizenmaier, K. (2010). Protein kinase D controls actin polymerization and cell motility through phosphorylation of cortactin. *J Biol Chem* **285**, 18672-83.

Eiseler, T., Kohler, C., Nimmagadda, S. C., Jamali, A., Funk, N., Joodi, G., Storz, P. and Seufferlein, T. (2012). Protein kinase D1 mediates anchorage-dependent and -independent growth of tumor cells via the zinc finger transcription factor Snail1. *J Biol Chem* **287**, 32367-80.

Eiseler, T., Wille, C., Koehler, C., Illing, A. and Seufferlein, T. (2015). Protein kinase D2 assembles a multiprotein complex at the Trans-Golgi-network to regulate matrix metalloproteinase secretion. *J Biol Chem*.

Eiseler, T., Wille, C., Koehler, C., Illing, A. and Seufferlein, T. (2016). Protein Kinase D2 Assembles a Multiprotein Complex at the Trans-Golgi Network to Regulate Matrix Metalloproteinase Secretion. *J Biol Chem* **291**, 462-77.

Geffrotin, C., Horak, V., Crechet, F., Tricaud, Y., Lethias, C., Vincent-Naulleau, S. and Vielh, P. (2000). Opposite regulation of tenascin-C and tenascin-X in MeLiM swine heritable cutaneous malignant melanoma. *Biochim Biophys Acta* **1524**, 196-202.

Gradiz, R., Silva, H. C., Carvalho, L., Botelho, M. F. and Mota-Pinto, A. (2016). MIA PaCa-2 and PANC-1 - pancreas ductal adenocarcinoma cell lines with neuroendocrine differentiation and somatostatin receptors. *Sci Rep* **6**, 21648.

Han, Y., Huang, C., Sun, X., Xiang, B., Wang, M., Yeh, E. T., Chen, Y., Li, H., Shi, G., Cang, H. et al. (2010). SENP3-mediated de-conjugation of SUMO2/3 from promyelocytic leukemia is correlated with accelerated cell proliferation under mild oxidative stress. *J Biol Chem* **285**, 12906-15.

He, S., McPhaul, C., Li, J. Z., Garuti, R., Kinch, L., Grishin, N. V., Cohen, J. C. and Hobbs, H. H. (2010). A sequence variation (I148M) in PNPLA3 associated with nonalcoholic fatty liver disease disrupts triglyceride hydrolysis. *J Biol Chem* **285**, 6706-15.

Hofmann, I., Kuhn, C. and Franke, W. W. (2008). Protein p0071, a major plaque protein of non-desmosomal adhering junctions, is a selective cell-type marker. *Cell Tissue Res* **334**, 381-99.

Hofmann, I., Schlechter, T., Kuhn, C., Hergt, M. and Franke, W. W. (2009). Protein p0071 - an armadillo plaque protein that characterizes a specific subtype of adherens junctions. *J Cell Sci* **122**, 21-4.

Housley, G. D., Morton-Jones, R., Vlajkovic, S. M., Telang, R. S., Paramananthasivam, V., Tadros, S. F., Wong, A. C., Froud, K. E., Cederholm, J. M., Sivakumaran, Y. et al. (2013). ATP-gated ion channels mediate adaptation to elevated sound levels. *Proc Natl Acad Sci U S A* **110**, 7494-9.

Irie, A., Harada, K., Araki, N. and Nishimura, Y. (2012). Phosphorylation of SET protein at Ser171 by protein kinase D2 diminishes its inhibitory effect on protein phosphatase 2A. *PLoS One* **7**, e51242.

Jablonski, A. M., Lamitina, T., Liachko, N. F., Sabatella, M., Lu, J., Zhang, L., Ostrow, L. W., Gupta, P., Wu, C. Y., Doshi, S. et al. (2015). Loss of RAD-23 Protects Against Models of Motor Neuron Disease by Enhancing Mutant Protein Clearance. *J Neurosci* **35**, 14286-306.

Kasimiotis, H., Myers, M. A., Argentaro, A., Mertin, S., Fida, S., Ferraro, T., Olsson, J., Rowley, M. J. and Harley, V. R. (2000). Sex-determining region Y-related protein SOX13 is a diabetes autoantigen expressed in pancreatic islets. *Diabetes* **49**, 555-61.

Keil, R., Kiessling, C. and Hatzfeld, M. (2009). Targeting of p0071 to the midbody depends on KIF3. *J Cell Sci* **122**, 1174-83.

Kinsey, M., Smith, R., Iyer, A. K., McCabe, E. R. and Lessnick, S. L. (2009). EWS/FLI and its downstream target NR0B1 interact directly to modulate transcription and oncogenesis in Ewing's sarcoma. *Cancer Res* **69**, 9047-55.

Landers, J. E., Melki, J., Meininger, V., Glass, J. D., van den Berg, L. H., van Es, M. A., Sapp, P. C., van Vught, P. W., McKenna-Yasek, D. M., Blauw, H. M. et al. (2009). Reduced expression of the Kinesin-Associated Protein 3 (KIFAP3) gene increases survival in sporadic amyotrophic lateral sclerosis. *Proc Natl Acad Sci U S A* **106**, 9004-9.

Lefave, C. V., Squatrito, M., Vorlova, S., Rocco, G. L., Brennan, C. W., Holland, E. C., Pan, Y. X. and Cartegni, L. (2011). Splicing factor hnRNPH drives an oncogenic splicing switch in gliomas. *EMBO J* **30**, 4084-97.

Makarenko, I. G., Meguid, M. M. and Ugrumov, M. V. (2002). Distribution of serotonin 5-hydroxytriptamine 1B (5-HT(1B)) receptors in the normal rat hypothalamus. *Neurosci Lett* **328**, 155-9.

Medvetz, D. A., Khabibullin, D., Hariharan, V., Ongusaha, P. P., Goncharova, E. A., Schlechter, T., Darling, T. N., Hofmann, I., Krymskaya, V. P., Liao, J. K. et al. (2012). Folliculin, the product of the Birt-Hogg-Dube tumor suppressor gene, interacts with the adherens junction protein p0071 to regulate cell-cell adhesion. *PLoS One* **7**, e47842.

Minoura, I., Takazaki, H., Ayukawa, R., Saruta, C., Hachikubo, Y., Uchimura, S., Hida, T., Kamiguchi, H., Shimogori, T. and Muto, E. (2016). Reversal of axonal growth defects in an extraocular fibrosis model by engineering the kinesin-microtubule interface. *Nat Commun* **7**, 10058.

Mori, M., Mahoney, J. E., Stupnikov, M. R., Paez-Cortez, J. R., Szymaniak, A. D., Varelas, X., Herrick, D. B., Schwob, J., Zhang, H. and Cardoso, W. V. (2015). Notch3-Jagged signaling controls the pool of undifferentiated airway progenitors. *Development* **142**, 258-67.

Rudinskiy, N., Grishchuk, Y., Vaslin, A., Puyal, J., Delacourte, A., Hirling, H., Clarke, P. G. and Luthi-Carter, R. (2009). Calpain hydrolysis of alpha- and beta2-adaptins decreases clathrin-dependent endocytosis and may promote neurodegeneration. *J Biol Chem* **284**, 12447-58.

Scharfmann, R., Pechberty, S., Hazhouz, Y., von Bulow, M., Bricout-Neveu, E., Grenier-Godard, M., Guez, F., Rachdi, L., Lohmann, M., Czernichow, P. et al. (2014).

Development of a conditionally immortalized human pancreatic beta cell line. *J Clin Invest* **124**, 2087-98.

Smirnova, N. F., Schamberger, A. C., Nayakanti, S., Hatz, R., Behr, J. and Eickelberg, O. (2016). Detection and quantification of epithelial progenitor cell populations in human healthy and IPF lungs. *Respir Res* **17**, 83.

Traynor, B. J., Nalls, M., Lai, S. L., Gibbs, R. J., Schymick, J. C., Arepalli, S., Hernandez, D., van der Brug, M. P., Johnson, J. O., Dillman, A. et al. (2010). Kinesin-associated protein 3 (KIFAP3) has no effect on survival in a population-based cohort of ALS patients. *Proc Natl Acad Sci U S A* **107**, 12335-8.

Whelan, S. A., Dias, W. B., Thiruneelakantapillai, L., Lane, M. D. and Hart, G. W. (2010). Regulation of insulin receptor substrate 1 (IRS-1)/AKT kinase-mediated insulin signaling by O-Linked beta-N-acetylglucosamine in 3T3-L1 adipocytes. *J Biol Chem* **285**, 5204-11.

Wille, C., Kohler, C., Armacki, M., Jamali, A., Gossele, U., Pfizenmaier, K., Seufferlein, T. and Eiseler, T. (2014). Protein kinase D2 induces invasion of pancreatic cancer cells by regulating matrix metalloproteinases. *Mol Biol Cell* **25**, 324-36.

Wohlfert, E. A., Gorelik, L., Mittler, R., Flavell, R. A. and Clark, R. B. (2006). Cutting edge: deficiency in the E3 ubiquitin ligase Cbl-b results in a multifunctional defect in T cell TGF-beta sensitivity in vitro and in vivo. *J Immunol* **176**, 1316-20.

Xiaojun, W., Yan, L., Hong, X., Xianghong, Z., Shifeng, L., Dingjie, X., Xuemin, G., Lijuan, Z., Bonan, Z., Zhongqiu, W. et al. (2016). Acetylated alpha-Tubulin Regulated by N-Acetyl-Seryl-Aspartyl-Lysyl-Proline(Ac-SDKP) Exerts the Anti-fibrotic Effect in Rat Lung Fibrosis Induced by Silica. *Sci Rep* **6**, 32257.

Zhao, X., Kuja-Panula, J., Rouhiainen, A., Chen, Y. C., Panula, P. and Rauvala, H. (2011). High mobility group box-1 (HMGB1; amphoterin) is required for zebrafish brain development. *J Biol Chem* **286**, 23200-13.

Zheng, H., Qian, J., Varghese, B., Baker, D. P. and Fuchs, S. (2011). Ligand-stimulated downregulation of the alpha interferon receptor: role of protein kinase D2. *Mol Cell Biol* **31**, 710-20.